Inorg. Chem. **2004**, *43*, 5613–5629

Red Shifting Due to Nonplanarity in Alkylporphyrins: Solid-State Polarized UV–Vis Spectra and ZINDO Calculations of Two Nickel(II)octaethylporphyrins

Jeremy S. Evans and Ronald L. Musselman*

Department of Chemistry, Franklin and Marshall College, Lancaster, Pennsylvania 17604

Received March 9, 2004

We present the first demonstration of red shifting upon nonplanarity in alkylporphyrins using two pure conformations having known structures with identical substituents. The traditional view about the relationship of spectral red shifting to nonplanar deformation in porphyrins has been that the deformation from planar to nonplanar forms is in itself the cause of the shifting, but recently this view has been challenged. Among the new arguments is that the substituents required to effect conformational change also bring about nuclear rearrangements in the porphyrin complex which is the actual cause of the red shifting. Octaethylporphyrinatonickel(II), however, exists in both planar and ruffled forms which are determined only by the crystal structure, thus making the issue of different substituents moot. Using a polarized specular reflectance UV–vis microspectrophotometer, we have obtained polarized spectra of pure, solid samples of both forms of NiOEP. We find Soret band red shifting in the solid state that is much larger than previous reports of solution spectra and also report Q-band red shifting. We performed ZINDO calculations on monomers and dimers of both forms of NiOEP, based upon reported structures, and have reproduced the reported solution transition energies and our solid-state spectra as well as the red shifts that we and others have found experimentally. We conclude that, at least in this system, red shifting does indeed result primarily from conformation changes in the porphyrin.

Metalloporphyrins are of interest because of their broad biological presence,[1,2] including light-gathering processes,[3] metal-catalyzed reductions,[4–7] and semiconductive properties.[8–10] Metal-free porphyrin derivatives are also found widely in natural systems, including, in the open ring form, as the active site in the plant growth regulators phytochromes.[11,12] Both crystal environments[13–15] and substituents on the macrocycle[16–18] may affect the structures of porphyrins, leading to doming, ruffling saddling, and other deformation of the planar ring which may lead to changes in reactive behavior.[19,20] Numerous reports show experimental evidence for modified reactivity in biological systems due to changes in the conformation of the complex.[21–26] Associ-

* Author to whom correspondence should be addressed. E-mail: ronald.musselman@fandm.edu.

(1) Dolphin, D.; James, B. R. In *ACS Symposium Series;* Ed.; American Chemical Society: Washington, DC, 1983; p 99.
(2) *Metals in Biological Systems;* Kendrick, M. J.; May, M. T.; Plishka, M. J.; Bobinson, K. D. Ellis Horwood: New York, 1992.
(3) Wagner, R. W.; Ruffing, J.; Breakwell, B. V.; Lindsey, J. S. *Tetrahedron Lett.* **1991**, *32*, 1703.
(4) Fuhrhop, J.-H.; Mauzerall, D. *J. Am. Chem. Soc.* **1969**, *91*, 4174.
(5) Kadish, K. M.; Franzen, M. M.; Han, B. C.; Araullo-McAdams, C.; Sazou, D. *J. Am. Chem. Soc.* **1991**, *113*, 512.
(6) Balch, A. L.; Noll, B. C.; Olmstead, M. M.; Phillips, S. L. *Inorg. Chem.* **1996**, *35*, 6495.
(7) Gunter, M. J.; Turner, P. *Coord. Chem. Rev.* **1991**, *108*, 115.
(8) Armstrong, N. R. *J. Porphyrins Phthalocyanines* **2000**, *4*, 414.
(9) Murata, K.; Liou, K. K.; Thompson, J. A.; McGhee, E. M.; Rende, D. E.; Ellis, D. E.; Musselman, R. L.; Hoffman, B. M.; Ibers, J. A. *Inorg. Chem.* **1997**, *36*, 3363.
(10) Liang, X.; Flores, S.; Ellis, D. E.; Hoffman, B. M.; Musselman, R. L. *J. Chem. Phys.* **1991**, *95*, 403.
(11) Quail, P. H. *Philos. Trans. R. Soc. London B.* **1983**, *303*, 387.
(12) Mas, P.; Devlin, P. F.; Panda, S.; Kay, S. A. *Nature* **2000**, *408*, 207.
(13) Meyer, E. F. J. *Acta Crystallogr.* **1972**, *B28*, 2162.
(14) Cullen, D. L.; Meyer, E. F. J. *J. Am. Chem. Soc.* **1974**, *96*, 2095.
(15) Brennan, T. D.; Scheidt, W. R.; Shelnutt, J. A. *J. Am. Chem. Soc.* **1988**, *110*, 3919.
(16) Haddad, R. E.; Gazeau, S.; Pecaut, J.; Marchon, J.-C.; Medforth, C. J.; Shelnutt, J. A. *J. Am. Chem. Soc.* **2003**, *125*, 1253.
(17) Prendergast, K.; Spiro, T. G. *J. Am. Chem. Soc.* **1992**, *114*, 3793.
(18) Medforth, C. J.; Senge, M. O.; Smith, K. M.; Sparks, L. D.; Shelnutt, J. A. *J. Am. Chem. Soc.* **1992**, *114*, 9859.
(19) Kadish, K. M.; Lin, M.; Caemelbecke, E. V.; De Stefano, G.; Medforth, C. J.; Nurco, D. J.; Nelson, N. Y.; Krattinger, B.; Muzzi, C. M.; Jaquinod, L.; Xu, Y.; Shyr, D. C.; Smith, K. M.; Shelnutt, J. A. *Inorg. Chem.* **2002**, *41*, 6673
(20) Shelnutt, J. A.; Oritz, V. *J. Phys. Chem.* **1985**, *89*, 4733.
(21) Barkigia, K. M.; Chantranupong, L.; Smith, K. M.; Fajer, J. *J. Am. Chem. Soc.* **1988**, *110*, 7566.

10.1021/ic0496931 CCC: $27.50
Published on Web 08/12/2004

ated with changes in conformation are well-documented red-shifts of both the Q and Soret (B) electronic absorption bands in such systems.[16,22,24,27−31] The first example of red-shifting being related to structure was in the zinc-containing complexes ZnOEP and ZnTPOEP (TPOEP = tetraphenyloctaethylporphyrin).[21] The former is planar and the latter is highly puckered, exhibiting a Q red-shift of 1.87 kcm^{-1} from ZnOEP. NiTPP (TPP = tetraphenylporphyrin), which exists as a mixture of planar and nonplanar forms in a carbon disulfide solution, has a Soret band at 424 nm but highly nonplanar Ni *meso*-tetra-adamantylporphyrin has its Soret band at 478 nm, a 54 nm, or 2.66 kcm^{-1}, red shift.[22] Red-shifting has also been demonstrated upon ruffling in a series of Fe(II) basket-handle porphyrins.[27] There is some counterevidence on the relationship of nonplanarity to red shifting in, for example, Fe(II) porphyrins.[32] If the red-shifting is indeed evidence of nonplanar conformations, spectral probes of biological reactions could determine the planarity of associated porphyrins.

In the past few years there has been a great deal of discussion about the cause of the red shifting in nonplanar porphyrins relative to their planar counterparts. The traditional position documented by Shelnutt and many others[16,27−29,33−35] is that the change in conformation itself is the cause of the red shifting, but in 1995 DiMagno et al. proposed[36] that there is a negligible effect on spectra by ruffling and that the red shifting is instead due to the effects of the different substituents used to obtain the different structures. The first response was a rebuttal five years later by Ghosh et al.[28] who used density functional theory (DFT) calculations of two forms of nonplanar zinc porphyrins to show that indeed there was significant red shifting in two nonplanar forms of a zinc porphyrin compared with its planar form, apparently due to the destabilizing of the HOMO's in the nonplanar forms. They also suggested that DiMagno et al.'s results had been due to shortcomings in their semi-empirical methods. The next year, DiMagno et al. responded[37] by reiterating that substituents provide conformational consequences in addition to nonplanarity, and it is these changes such as in bond lengths and angles, which they referred to as in-plane nuclear reorganizations (IPNR's), that lead to the red shifting. They also suggested calculation errors on the part of Ghosh et al. Ghosh responded in 2002[32] that upon reinvestigating the issue with time-dependent density functional theory (TDDFT) calculations, they reported that DiMagno et al. were indeed correct regarding their claim that ruffling did not in itself cause red shifting and they extended that same conclusion to saddled porphyrins. Additionally, they suggested that interaction between a metal d_{xy} orbital and a porphyrin a_{2u} orbital is especially effective at raising the a_{2u} HOMO-1 level, thus leading to the red shift.[32] Shelnutt and co-workers were prompted by these developments to pursue more deeply the nature of the effect of structural perturbations on the electronic spectra of porphyrins. In 2003, they reported[16] that the basic experimental evidence still confirms large red shifts due to nonplanarity and that the deformations due to a limited set of normal vibrational modes contribute to spectral red shifting as well.

Octaethylporphyrinatonickel(II) (NiOEP) provides a clear case of conformational change without the changed substituents which have led to the invocation of IPNR's, since NiOEP exists in both planar (*plan*) and ruffled (*ruf)* forms depending upon its crystal structure.[13−15] Side views of the *plan* and *ruf* forms are shown on the left side of Figure 1. The *plan* form, in the triclinic B crystal,[15] is very close to planar, with only a 2° tilt of the pyrrole rings and has the ethyl groups on one-half of the macrocycle up and those on the other half down. The *ruf* form, in the tetragonal crystal,[13] is clearly nonplanar; opposite pyrrole rings are tilted by 28.4° with respect to each other and the ethyl groups alternate in pairs up and down around the structure. The pyrrole rings are planar and the structure matches the lowest-frequency B_{1u} deformation (1 B_{1u}) as characterized by Shelnutt et al.[16] Both forms have an essentially planar NiN_4 core.

UV−visible spectra of NiOEP have been obtained in solution[22,24,25,29,30,38−42] and vapor phase,[43] but the solution appears to consist of a mixture of *plan* and *ruf* forms,[25,29,31] although one report found only the *plan* form in solution.[42] The ratio of the *plan* to non-*plan* forms appears to change with temperature, but it is not clear which way: one report has it increasing with increasing temperature[29] and another

(22) Jentzen, W.; Simpson, M. C.; Hobbs, J. D.; Song, X.; Ema, T.; Nelson, N. Y.; Medforth, C. J.; Smith, K. M.; Veyrat, M.; Mazzanti, M.; Ramasseul, R.; Marchon, J. C.; Takeuchi, T.; Goddard, W. A.; Shelnutt, J. A. *J. Am. Chem. Soc.* **1995**, *117*, 11085.
(23) Jentzen, W.; Unger, E.; Karvounis, G.; Shelnutt, J. A.; Dreybrodt, W.; Schweitzer-Stenner, R. *J. Phys. Chem.* **1996**, *100*, 14184.
(24) Cupane, A.; Leone, M.; Lorenzo, C.; Gilch, H.; Dreybrodt, W.; Unger, E.; Schweitzer-Stenner, R. *J. Phys. Chem.* **1996**, *100*, 14192.
(25) Schweitzer-Stenner, R.; Stichternath, A.; Dreybrodt, W.; Jentzen, W.; Song, X.-Z.; Shelnutt, J. A.; Nielsen, O. F.; Medforth, C. J.; Smith, K. M. *J. Chem. Phys.* **1997**, *107*, 1794.
(26) Furenlid, L. R.; Renner, M. W.; Smith, K. M. *J. Am. Chem. Soc.* **1990**, *112*, 1634.
(27) Picaud, T.; Le Moigne, C.; Loock, B.; Momenteau, M.; Desbois, A. *J. Am. Chem. Soc.* **2003**, *125*, 11616.
(28) Parusel, A. B. J.; Wandimagegn, T.; Ghosh, A. *J. Am. Chem. Soc.* **2000**, *122*, 6371.
(29) Alden, R. G.; Crawford, B. A.; Doolen, R.; Ondrias, M. R.; Shelnutt, J. A. *J. Am. Chem. Soc.* **1989**, *111*, 2070.
(30) Choi, S. H.; Phillips, J. A.; Ware, W.; Wittschieben, C.; Medforth, C. J.; Smith, K. M. *Inorg. Chem.* **1994**, *33*, 3873.
(31) Czernuszewicz, R. S.; Macor, K. A.; Li, X.-Y.; Kincaid, J. R.; Spiro, T. G. *J. Am. Chem. Soc.* **1989**, *111*, 3860.
(32) Ryeng, H.; Ghosh, A. *J. Am. Chem. Soc.* **2002**, *124*, 8099.
(33) Senge, M. O. In *The Porphyrin Handbook;* Kadish, K. M., Smith, K. M., Guilard, R., Eds.; Academic Press: Boston, 2000; p 239.
(34) Shelnutt, J. A.; Song, X.-Z.; Ma, J.-G.; Jentzen, W.; Medforth, C. J. *J. Chem. Soc. Rev.* **1998**, *27*, 31.
(35) Ravikanth, M.; Chandrashekar, T. K. *Struct. Bonding (Berlin)* **1995**, *82*, 105.
(36) DiMagno, S. G.; Wertsching, A. K.; Ross, C. R. *J. Am. Chem. Soc.* **1995**, *117*, 8279.
(37) Wertsching, A. K.; Koch, A. S.; DiMagno, S. G. *J. Am. Chem. Soc.* **2001**, *123*, 3932.
(38) Stanley, K. D.; Luo, L.; Lopez de la Vega, R.; Quirke, J. M. E. *Inorg. Chem.* **1993**, *32*, 1233.
(39) Bobinger, U.; Schweitzerstenner, R.; Dreybrodt, W. *J. Phys. Chem.* **1991**, *95*, 7625.
(40) Arnold, D. P.; James, D. A. *J. Org. Chem.* **1997**, *62*, 3460.
(41) Eastwood, D.; Gouterman, M. *J. Mol. Spectrosc.* **1970**, *35*, 359.
(42) Spaulding, L. D.; Chang, C. C.; Yu, N.-T.; Felton, R. H. *J. Am. Chem. Soc.* **1975**, *97*, 2517.
(43) Edwards, L.; Dolphin, D. H.; Gouterman, M. *J. Mol. Spectrosc.* **1970**, *35*, 90.

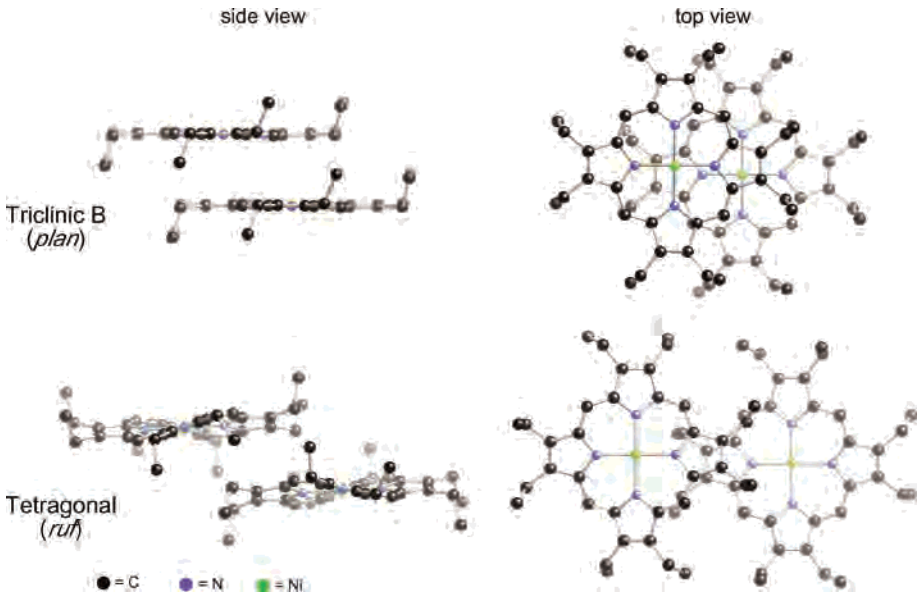

Figure 1. Side and top views of pairs of molecules in two forms of NiOEP crystals. Triclinic B data from ref 15 and tetragonal data from ref 13.

has it decreasing with increasing temperature.[31] A great deal of effort has been expended in identifying the two forms of the complex in solution through both UV absorption and resonance Raman spectroscopy[15,24,29,42] including the development of Shelnutt's normal-coordinate structural decomposition (NSD)[16,44,45] for determining the type and degree of conformational distortion in porphyrins. Red shifts of the Soret transition in the *ruf* form of NiOEP in solution have been reported to be 857 cm^{-1} [29] and 220 cm^{-1}.[24] The halfwidth of this transition in a $CHCl_3$ solution is 1320 cm^{-1};[40] deconvolution of peaks separated by much less than the half-width is difficult, and this partially explains the uncertainty in the degree of red shift. In addition, it is difficult to evaluate the amount of *plan* or *ruf* when both are present in solution and when it has not been possible to obtain the spectrum of either of the pure conformations in solution.

Obtaining spectra of the two conformers in their crystalline states would be desirable in order to clearly identify spectra from the two forms. Standard transmission absorption UV−vis, however, would be difficult since the molecules have very high extinction coefficients. For a material with an absorptivity of 100000 M^{-1} cm^{-1} (as with NiOEP) the sample thickness would need to be less than 2×10^{-5} mm. On the other hand, highly absorbing samples are also highly reflecting, and specular (mirrorlike) reflectance from the natural faces of single crystals is measurable. Using a polarized specular reflectance UV−vis microspectrophotometer, we have been able to observe in-plane spectra for the triclinic B crystal and both in-plane and out-of-plane spectra for the tetragonal crystal. We find Soret band *plan*−*ruf* red shifting in the solid state that is much larger than previous reports of such shifting in solution,[24,29] and we also report Q-band red shifting.

Table 1. Crystal Parameters

	tetragonal		triclinic B		triclinic A
parameter	literature[13]	found	literature[15]	found	literature[14]
a, Å	14.93 ± 0.01	14.85 ± 0.1	13.302 (6)	13.21 ± 0.1	9.924(3)
b, Å	14.93 ± 0.01		13.342(11)	13.42 ± 0.1	10.564(3)
c, Å	13.84 ± 0.01	13.86 ± 0.1	4.802(2)		7.617(2)
α, deg	90		92.21(2)		97.66(2)
β, deg	90	89.4 ± 0.7	93.52(4)		109.47(3)
γ, deg	90		113.43(6)	113.67 ± 0.7	92.35(3)

Our plan in this paper is to present the solid-state spectra and then discuss calculations vis-à-vis experiment for monomers (solution) and then dimers (solid-state). We will also discuss solid-state perturbations and causes of *plan*−*ruf* red shifting.

Experimental Section

Preparation. NiOEP was purchased from Aldrich Chemical Co. as a 97% pure crystalline solid. The sample contained almost exclusively the tetragonal form, having a square-bipyramidal structure.[13] Crystals were selected based upon surface quality and were used without further purification for the tetragonal form studies. For the triclinic form, we followed the procedure for the triclinic A crystal:[14] a saturated solution was prepared in a 1:1 pyridine−dioxane mixture at 85 °C and cooled to room temperature over a period of 115 h. A mixture of tetragonal and triclinic crystals resulted; they were distinguishable through their crystal morphologies: the triclinic were elongated needles.[14,15] The triclinic crystals selected were determined to have the triclinic B structure[15] through single-crystal 0-level Weissenberg X-ray photos; Table 1 lists our experimental values and literature crystal parameters. The tetragonal crystals were confirmed with the same procedure.

Single-Crystal Polarized Reflectance Spectroscopy. Polarized specular reflectance spectra were obtained with a new instrument which is a major upgrade of our previous reflectance instrument.[46,47]

(44) Jentzen, W.; Song, X. Z.; Shelnutt, J. A. *J. Phys. Chem. B* **1997**, *101*, 1684.
(45) Shelnutt, J. A. In *The Porphyrin Handbook;* Kadish, K. M., Ed.; Academic Press: Boston, 2000; p 167.
(46) Desjardins, S. R.; Penfield, K. W.; Cohen, S. L.; Musselman, R. L.; Solomon, E. I. *J. Am. Chem. Soc.* **1983**, *105*, 4590.
(47) Cornelius, J. B.; Trapp, R. M.; Delord, T. J.; Fronczek, F. R.; Watkins, S. F.; Orosz, J. J.; Musselman, R. L. *Inorg. Chem.* **2003**, *42*, 3026.

The current instrument is a single beam, wide range, fast spectrophotometer. Light sources are a xenon arc lamp and a tungsten−halogen lamp, the polarizer is a MgF_2 Rochon prism, optics are spherical and planar reflectors with an Ealing Optics reflecting objective. Image beam size is 30 μ (0.030 mm), sample and reference mirror motions are computer controlled, UV and visible dispersion is through an Acton Research SpectraPro 275 spectrograph, and detection is with a Princeton Instruments 1152 × 296 EEV (English Electric Valve) CCD (Charge-Coupled Device), maintained at 110 K. All instrument control and data collection is through a Macintosh computer. Spectra were recorded from selected highly reflective natural faces of both crystal morphologies. The average of 50 spectra is reported in each case; the exposure time for each ranged from 0.01 to 20 s, depending on the spectral region. The data were corrected for percent reflectivity relative to a NIST standard mirror.

Specular reflectance data, while interesting and somewhat informative in themselves, are most useful in the context here upon transformation into absorbance data via a Kramers−Kronig transformation.[48,49] For Kramers−Kronig analysis which formally includes integration over an infinite range of energies, reflectivities beyond our experimental region were estimated in the infrared region and below to be equal to the lowest-energy experimental measurements and were approximated in the vacuum ultraviolet and beyond so as to produce baselines approaching zero absorbance in regions having no absorbance in solution spectra. Examples of such "effective transitions" are discussed in a recent paper.[47] Deconvolution was carried out with an interactive Gaussian and Lorentzian program ("FastGauss"[50]) on a Macintosh computer.

Crystal Morphology, Structure, and Polarization Orientations. Since specular reflectance spectroscopy is performed on the natural surfaces of single crystals, we had to determine the orientation of molecules with respect to the morphology of each crystal form used. We were able to do this through single-crystal X-ray film work and a technique reported earlier[51] to coordinate reciprocal axes and the crystal morphology. The tetragonal crystal used for reflectance spectra had outer dimensions of 0.50 × 0.50 × 0.50 mm, and the face from which spectra were obtained was 0.50 × 0.030 mm. The triclinic crystal used had dimensions ~0.060 × 0.030 × 0.50 mm, and the face used for reflectance had dimensions of 0.030 × 0.50 mm.

Figure 2a shows the tetragonal form with its bicapped square-pyramidal morphology; the *c* axis is through the vertices. There is also a set of narrow side faces, (100), (010), ($\bar{1}$00), and (0$\bar{1}$0), and, due to the tetragonal symmetry, all of these side faces provide equivalent views of the molecules. The molecules in the tetragonal structure are bent in a ruffled (rather than saddle)[52] shape with the pyrrole rings twisted by 14.2° from the exactly planar NiN_4 center group.[13] We will define the planar directions relative to the square-planar NiN_4 group; the molecule has D_{2d} symmetry. The morphology and structure allow clear delineation of z from x,y polarization as can be seen visually in Figure 2a and also in Table 1 where squares of projection coefficients are listed. We obtained spectra from one of the side faces with the electric vector parallel to the crystallographic *c* axis for z-polarized spectra and perpendicular to c for the x,y-polarized spectra.

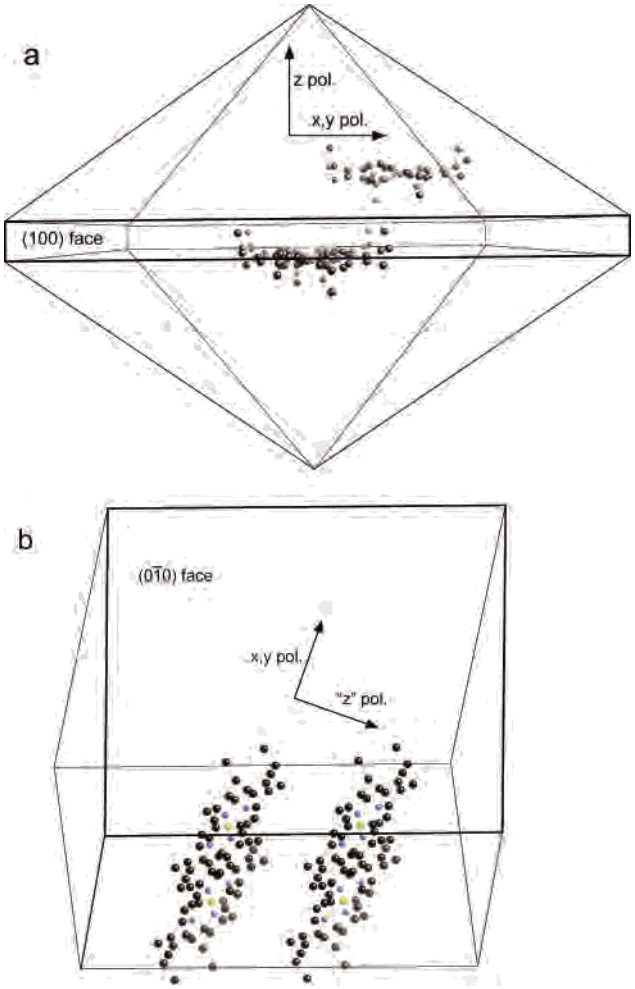

Figure 2. Crystal morphology of NiOEP crystals, showing selected molecules, viewed normal to face from which spectra were obtained, and polarization directions: (a) tetragonal and (b) triclinic B.

The planar cores in the tetragonal structure are parallel, and the molecules are moderately closely stacked. The pyrrole ring to the right of the nickel on one molecule lies over the pyrrole ring to the left of the nickel on the adjacent molecule, as seen in Figure 1. The interplanar distance of about 3.6 Å[13] allows for some degree of $\pi-\pi$ interaction between adjacent planes. Nickel atoms lie over spaces between two macrocycles in the adjacent layers so there is no Ni-π interaction.

The structure of the triclinic B crystal does not have the symmetrical morphology of the tetragonal crystal, but the individual NiOEP molecules do have a nearly planar structure except, of course, for the terminal methyl groups and the methylene hydrogens on the eight ethyl groups.[15] The complex has only a center of symmetry (in addition to an identity element) if the hydrogens are not considered,[15] giving it C_i symmetry. Although there are significant bond distance and angle departures from D_{4h} symmetry, the structure and near planarity make it close enough to D_{4h} that D_{4h} terminology would be better than C_i when comparing assignments with earlier studies[53−55] of porphyrins since C_i has only a_g and a_u symmetries available.

Figure 2b shows four molecules in a representation of the crystal morphology viewed normal to the (0$\bar{1}$0) face which presents the

(48) Anex, B. G. *Mol. Cryst.* **1966**, *1*, 1.
(49) Kronig, R. *J. Opt. Soc. Am.* **1926**, *12*, 547.
(50) Haddon, H.; Musselman, R. L. FastGauss, Franklin and Marshall College: 1992.
(51) Musselman, R. L.; Schneider, A. A. G. *Appl. Spectrosc.* **1987**, *41*, 106.
(52) Scheidt, W. R.; Lee, Y. J. *Struct. Bonding (Berlin)* **1987**, *64*, 1.
(53) Gouterman, M. *J. Chem. Phys.* **1959**, *30*, 1139.
(54) Gouterman, M. *J. Mol. Spectrosc.* **1961**, *6*, 138.
(55) Gouterman, M.; Wagniere, G. H.; Snyder, L. C. *J. Mol. Spectrosc.* **1963**, *11*, 108.

Table 2. Relative Contribution of the Molecular Polarizations to Each Spectrum

crystal/face	polarization	angle from spindle (c) axis (deg)	I_x coeff[a]	I_y coeff[a]	I_z coeff[a]
triclinic B/(0$\bar{1}$0)	xy	+42.0	0.83	0.16	0.00
triclinic B/(0$\bar{1}$0)	xyz = "z"	−48.0	0.01	0.06	0.92
tetragonal/(100)	xy	0.0	0.00	1.00	0.00
tetragonal/(100)	z	90.0	0.00	0.00	1.00

[a] I_a is calculated as the magnitude squared of the projection of the *a* molecular vector onto a vector parallel to the electric vector of light.

greatest degree of separation of the x, y, and the z directions. The projections of the x, y, and z molecular axes onto the (0$\bar{1}$0) face are at 40.3, 78.5, and −48.0°, respectively, from the *c* or spindle, axis with magnitudes of 0.912, 0.500, and 0.959. The orientation for the electric vector to obtain the greatest degree of z polarization was −48.0°; the x,y polarized spectrum was chosen as 42.0°, which is 90° off the z direction. The intensity components of the x, y, and z molecular directions are listed in Table 2. The polarization directions were based upon molecular orientations, as always in our specular reflectance work, rather than natural extinction directions because of the surface nature of the reflectance process.

The planes in the triclinic B crystal are closely stacked, with an interplanar distance of 3.44 Å but are shifted relative to each other so that the Ni−Ni distance is 4.80 Å and the angle between the Ni−Ni axis and each plane is 134.0°.[15] Nickel atoms on one plane lie over an edge of the pyrrole ring of an adjacent plane. Such relatively close stacking has resulted in significant red-shifting from solution values of transitions involving Ni p and d orbitals in tetracyanonickelate salts, and this effect has been also observed in the ZINDO modeling of those systems.[47, 56]

We thus have two very different cases: a ruffled molecule whose crystal structure allows clean separation of the polarizations with little apparent metal-π interplanar interaction and a planar molecule in a crystal which should provide 92% of the z polarization with a small mixture of x and y polarizations and with the possibility of observable metal-π interplanar interaction.

Semiempirical Calculations. Calculations of molecular orbital wave functions and eigenvalues and electronic state transitions were performed on single molecules and two-molecule aggregates of NiOEP in both the tetragonal and triclinic B structures using the Zerner-modified semiempirical INDO (Intermediate Neglect of Differential Overlap) method known as ZINDO.[57] We also calculated energies for porphyrinatonickel(II) (NiP) orbitals and "ZnOEP" orbitals, in which Zn was substituted for Ni in NiOEP structures, and flattened tetragonal NiOEP's in which all ring atoms are exactly planar. In the case of the latter, flattening was feasible since the principal 2-fold D_{2d} axis is coincident with the crystallographic *z* axis; we changed all core atoms to the *z* value for Ni and moved the ethyl groups in a corresponding manner. Once that was done, we locked the planar group and allowed the locations of the methylene hydrogens and the terminal methyl group on the ethyls to optimize using Molecular Mechanics in the CAChe suite of programs from Fujitsu.[58] We also expanded and contracted the flattened porphyrin core by 3% to test for bond length effects. All structures were derived from literature X-ray structure reports. The version of ZINDO we use here is contained in CAChe. It has been extremely successful in calculating theoretical electronic spectra of the dianion $Ni(CN)_4^{2-}$ [59] and several solid-state $Ni(CN)_4^{2-}$ salts[47,56] as well as numerous porphyrinic complexes.[60−62]

The ZINDO program in CAChe allows variation on several parameters. The parameters most commonly adjusted in transition metal complexes are the bonding parameters β_s, β_p, and β_d for the central metal.[63] β_s and β_p are set equal ("β_{sp}") and represent the amount of interaction between occupied s and p orbitals on the metal with atomic orbitals on adjacent atoms; β_d is correspondingly defined. Values which are more negative represent a greater interaction between the corresponding metal orbital(s) and the ligand orbitals. In previous studies in our laboratory[56,59] values of β_{sp} and β_d were optimized for $Ni(CN)_4^{2-}$ and its salts; we used similar methods on the molecules under study here. Little or no change resulted, however, from changes in the β_{sp} and β_d values from the default values of −1 and −41 eV, respectively, so these values were retained. Other studies of porphyrins have also used $\beta_{sp} = -1$ and $\beta_d = -41$ eV for Ni.[63]

Another adjustable parameter is the level of configuration interaction (CI). The CI process in ZINDO considers the effects of single-electron excitations from a set of filled orbitals to a set of virtual orbitals. The "CI level" is an integer representing the number of orbitals in each region used in the CI calculation. Since the ZINDO CI in CAChe includes only single excitations, the choice of CI level in this case affects only the state transitions and not the individual orbital energies or wave functions.[59] Variation of the CI level from CI = 10 to CI = 18 for single molecules produced only slight changes in the overall calculated spectra. At values below 10 some experimental transitions had no clear counterpart in the calculated spectra for the single-molecule *ruf* structure. Changes occurred gradually and slightly for both single-molecule structures as the CI level was increased from a value of 10: a transition at 32.00 kcm^{-1} with CI = 10 moved to 31.20 kcm^{-1} with CI = 18. We chose 14 as a reasonable CI level for single molecules. Common practice suggests that higher CI levels are less desirable only because of the increased calculation time. We found, however, that major deviations from the experimental result may occur if the CI level is raised above an optimal level.[59] For the aggregated sets of two molecules, we used the maximum value in the CAChe suite of CI = 22.

Spectroscopic Results

The polarized specular reflectance spectra of the two polarizations of the (0$\bar{1}$0) face of the triclinic B form of NiOEP are shown in Figure 3a. Upon transformation into absorbance values using the Kramers−Kronig algorithm, the reflectance spectra yield the absorbance spectra shown in Figure 3b. As noted in Table 2, the orientations of the molecules were such that the calculated "x,y" polarization

(56) Fronczek, F. R.; Delord, T. J.; Watkins, S. F.; Gueorguieva, P.; Stanley, G. G.; Zizza, A. S.; Cornelius, J. B.; Mantz, Y. A.; Musselman, R. L. *Inorg. Chem.* **2003**, *42*, 7026.
(57) Ridley, J.; Zerner, M. *Theor. Chim. Acta* **1973**, *32*, 111.
(58) Zerner, M. C. ZINDO (in CAChe), Fujitsu Limited: Beaverton, OR 97006, 2000.
(59) Mantz, Y. A.; Musselman, R. L. *Inorg. Chem.* **2002**, *41*, 5770.
(60) Edwards, W. D.; Weiner, B.; Zerner, M. C. *J. Am. Chem. Soc.* **1986**, *108*, 2196.
(61) Vitasovic, M.; Gouterman, M.; Linschitz, H. *J. Porphyrins Phthalocyanines* **2001**, *5*, 191.
(62) Mack, J.; Stillman, M. J. *Inorg. Chem.* **1997**, *36*, 413.
(63) Anderson, W. P.; Edwards, W. D.; Zerner, M. C. *Inorg. Chem.* **1986**, *25*, 2728.

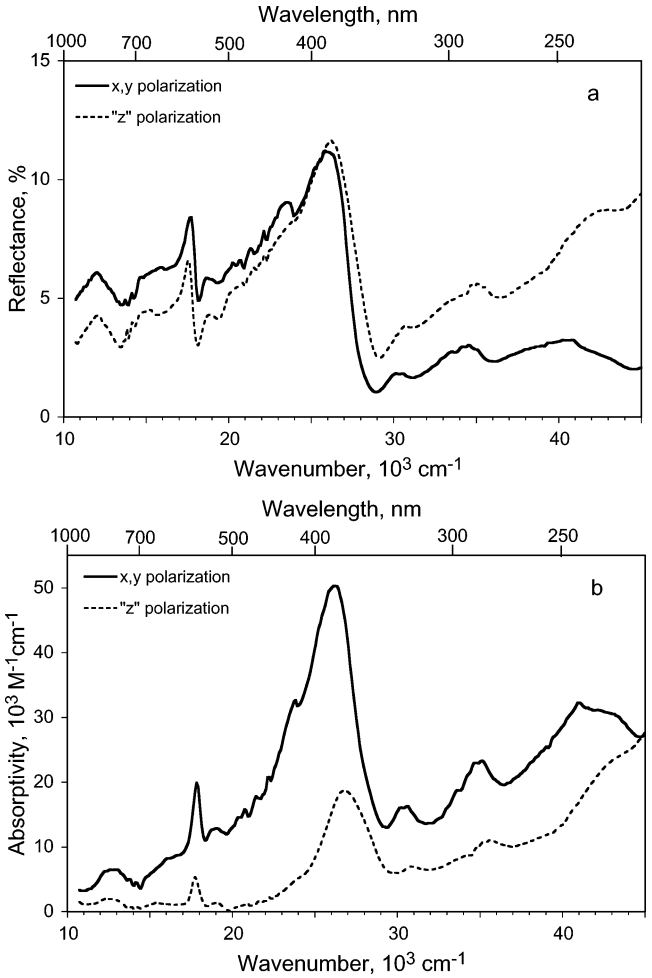

Figure 3. Polarized spectra for NiOEP triclinic B: (a) reflectance and (b) absorbance.

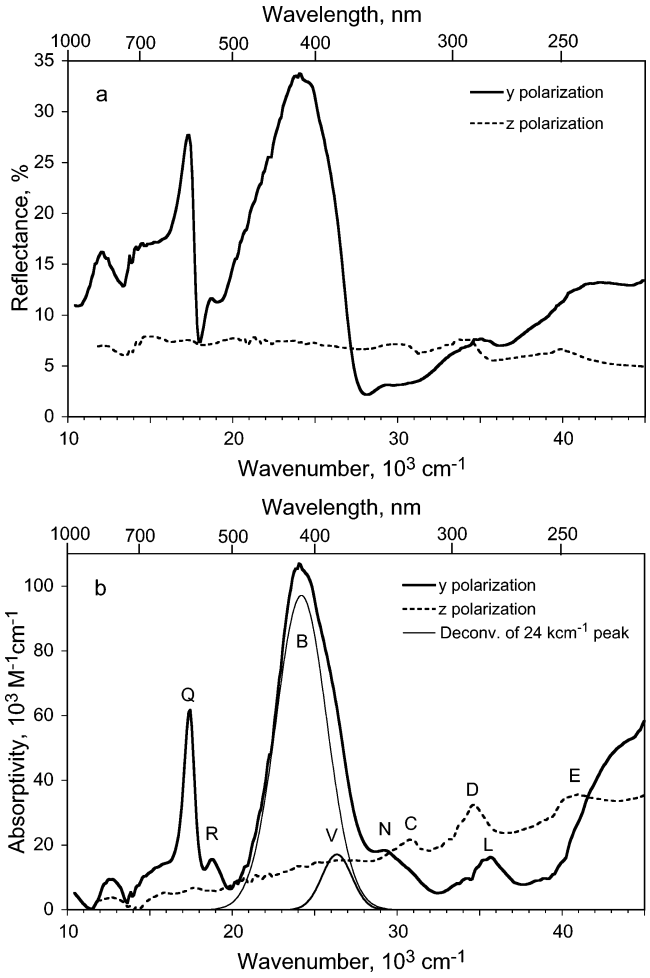

Figure 4. Polarized spectra for NiOEP tetragonal: (a) reflectance and (b) absorbance.

would be 83% x and 16% y and the "z" polarization 1% x, 6% y, and 92% z (rounding errors account for the less than 100% total). As may be seen from a cursory examination of the two absorbance spectra in Figure 3b, particularly in the 26 kcm^{-1} region, the "z" polarization peak seems to be about one-third the intensity of the corresponding peak in the x,y-polarized spectrum. Since from ZINDO calculations (vide infra) we do not expect any significant z-polarized transitions in this region, the intensity of this peak in the "z"-polarized spectrum should be primarily from the x and y contribution, about 7% of the total x- and y-polarized transition. The quite large transition is apparently due to a partial depolarization of the light as it traverses a very shallow layer of the crystal during the specular reflectance process, which is known to occur in crystals with lower than orthogonal symmetry.[64−66] This would cause x,y-polarized absorptions to partially appear in the z-polarized spectrum and for the corresponding peak in the x,y-polarized spectrum to be less intense than expected.

The reflectance spectra from the (100) face of the tetragonal form of NiOEP are shown in Figure 4a and they show clearly that the polarization directions are well separated as expected both from the calculated projections onto the (100) face and the orthogonal nature of the crystal as suggested in the previous paragraph. The transformed absorbance spectra in Figure 4b confirm the excellent dichroism of this crystal.

In Table 3 we have summarized these solid-state spectral values along with results from earlier vapor- and solution-phase studies.[24,29,43,67] Solution values for the B peak show that Shelnutt's reported *plan* B peak[29] is very close to Gouterman's undetermined-form solution peak,[67] suggesting that the two are equivalent. In addition, Shelnutt's *ruf* B peak is red-shifted by 857 cm^{-1}[29] from the *plan* peak, while Cupane's red shift is 220 cm^{-1}.[24] Our solid-state results show a greater spectral difference between the *plan* and *ruf* forms than either of these observations. The *plan* peak B is at 26.2 kcm^{-1} (close to the vapor-phase results),[43] and the *ruf* peak B is at 24.0 kcm^{-1}, for a red shift of 2200 cm^{-1}. This solid-state *plan*−*ruf* red shift is much larger than the half width of the NiOEP solution Soret transition which contains both *plan* and *ruf* forms.[40] At first glance, we suspect that our observed red shift is at least partially enhanced by the solid-state environment. We will revisit this issue after having presented ZINDO calculations on our solid-state model.

(64) Anex, B. G.; Fratini, A. V. *J. Mol. Spectrosc.* **1964**, *14*, 1.
(65) *Crystals and the polarizing microscope;* Hartshorne, N. H., Stuart, A. 3rd, Eds.; Arnold: London, 1960.
(66) Fratini, Ph.D. Dissertation, Yale University, 1966.
(67) Antipas, A.; Gouterman, M. *J. Am. Chem. Soc.* **1983**, *105*, 4896.

Table 3. Experimental and Calculated Spectral Data for NiOEP

		NiOEP									"ZnOEP"					
form	reference	$B_{(0,0)}$ wavel, nm	wave-num, kcm^{-1}	*p*−*r* red shift, kcm^{-1}	$Q_{(0,1)}$ wavel, nm	wave-num, kcm^{-1}	*p*−*r* red shift, kcm^{-1}	$Q_{(0,0)}$ wavel, nm	wave-num, kcm^{-1}	*p*−*r* red shift, kcm^{-1}	$B_{(0,0)}$ wavel, nm	wave-num, kcm^{-1}	*p*−*r* red shift, kcm^{-1}	$Q_{(0,0)}$ wavel, nm	wave-num, kcm^{-1}	*p*−*r* red shift, kcm^{-1}
						Experimental										
						Vapor										
undetermined form	Edwards et al.[43]	385	26.0		522	19.2		558	17.9							
						Solution (CH_2Cl_2)										
undetermined form	Gouterman et al.[67]	392	25.5		516	19.4		551	18.1							
plan	Barkigia et al.[21]													569	17.57	
plan	Shelnutt et al.[29]	393	25.44													
ruf	Shelnutt et al.[29]	407	24.59	0.86												
						Solid State										
triclinic B = *plan*	this work	382	26.2		526	19.1		559	17.9							
tetragonal = *ruf*	this work	417	24.0	2.20	532	18.8	0.30	575	17.4	0.50						
						Calculated										
						Monomer										
triclinic B = *plan*	this work	316[a]	31.64[a]					567[a]	17.62[a]			31.90			17.46	
tetragonal = *ruf*	this work	325	30.77	0.87				577	17.32	0.30		31.06	0.85		17.11	0.35
plan−*ruf*	Shelnutt et al.[29]			0.41						0.36						
						Dimer										
triclinic B = *plan*	this work	308	32.46					568	17.60							
tetragonal = *ruf*	this work	334	29.97	2.49				580	17.24	0.36						

[a] Average values of two transitions; individual values are listed in Table 5.

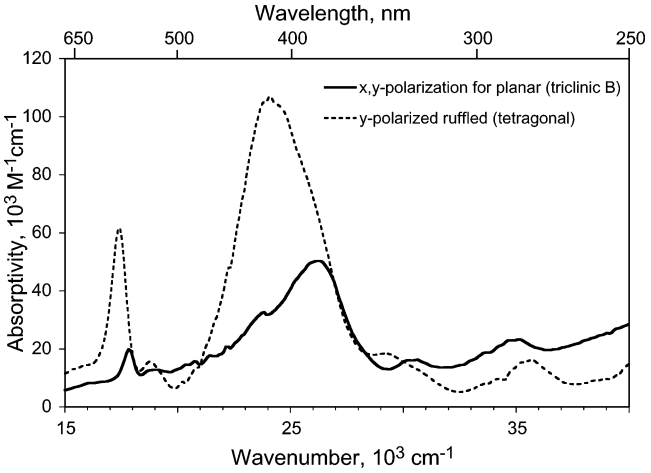

Figure 5. X,y-polarized experimental absorbance spectra for triclinic B and tetragonal NiOEP.

The Q(0,0) peaks are especially well defined: our *plan* Q(0,0) peak is at 17.9 kcm^{-1}, the same as the vapor-phase results,[43] and the equivalent *ruf* peak is at 17.4 kcm^{-1}, red-shifted by 500 cm^{-1}. The Q(0,1) peaks (designated as R in Figure 4b) are not as well defined, but the *plan* and *ruf* peaks are 1.2 kcm^{-1} and 1.4 kcm^{-1} higher, respectively, than the corresponding Q(0,0) values, comparable to Gouterman's difference of 1.3 kcm^{-1}.[43,67] They show a red shift of the *ruf* form of 300 cm^{-1}. Figure 5 shows the in-plane spectra for both the *plan* and *ruf* forms of NiOEP, illustrating the red-shifts of both prominent transitions. In addition to the red shifts, it is clear that the peak intensities for the *plan* form are significantly reduced from those for the *ruf* form which illustrates the effect of depolarization in the triclinic crystal as mentioned earlier.

Our solid-state *plan* results being very close to the vapor-state results[43] suggest that if the vapor form is planar and monomeric there is minimal perturbation in the triclinic B (*plan)* crystal form; countering this is the much larger *plan*−*ruf* red shift than previously reported that we find experimentally. We will report on ZINDO calculations of dimers of NiOEP in a later section to explore the extent of solid-state perturbations.

Calculations and Discussion

We will present the discussion in tandem with calculation results as we compare reported solution spectra with our calculated monomer transitions and our solid-state spectra with calculated dimer transitions. We will then examine the solid-state effects in order to relate our solid-state spectra to reported solution spectra and finally take a look at possible causes of red shifting in metalloakylporphyrins.

Monomers. The purpose of the monomer calculations is both to understand the orbital energies, wave functions, and transition energies in single NiOEP molecules and to provide a basis for the solid-state modeling calculations. The calculated results also provide a link to previous interpretations of porphyrin spectra. We place a greater emphasis on these calculations than on the dimer transitions because they are much simpler than the latter and provide a clear set of results for the purpose of transition assignments. Comparison with solution spectra is done with the understanding that Alden et al.[29] have reported that the porphyrin ring is less distorted in solution than in the tetragonal crystal, the latter being the conformation upon which our *ruf* calculations are based.

Energy Levels. Energy levels are of special interest because of the well-known relationship between the two lowest unfilled MO's and the two highest occupied MO's and their generation of both the Q and B, or Soret, transitions. In unsubstituted porphyrins, the two LUMO's are symmetry degenerate and the two HOMO's are accidentally degenerate. Configuration interaction between these four orbitals was

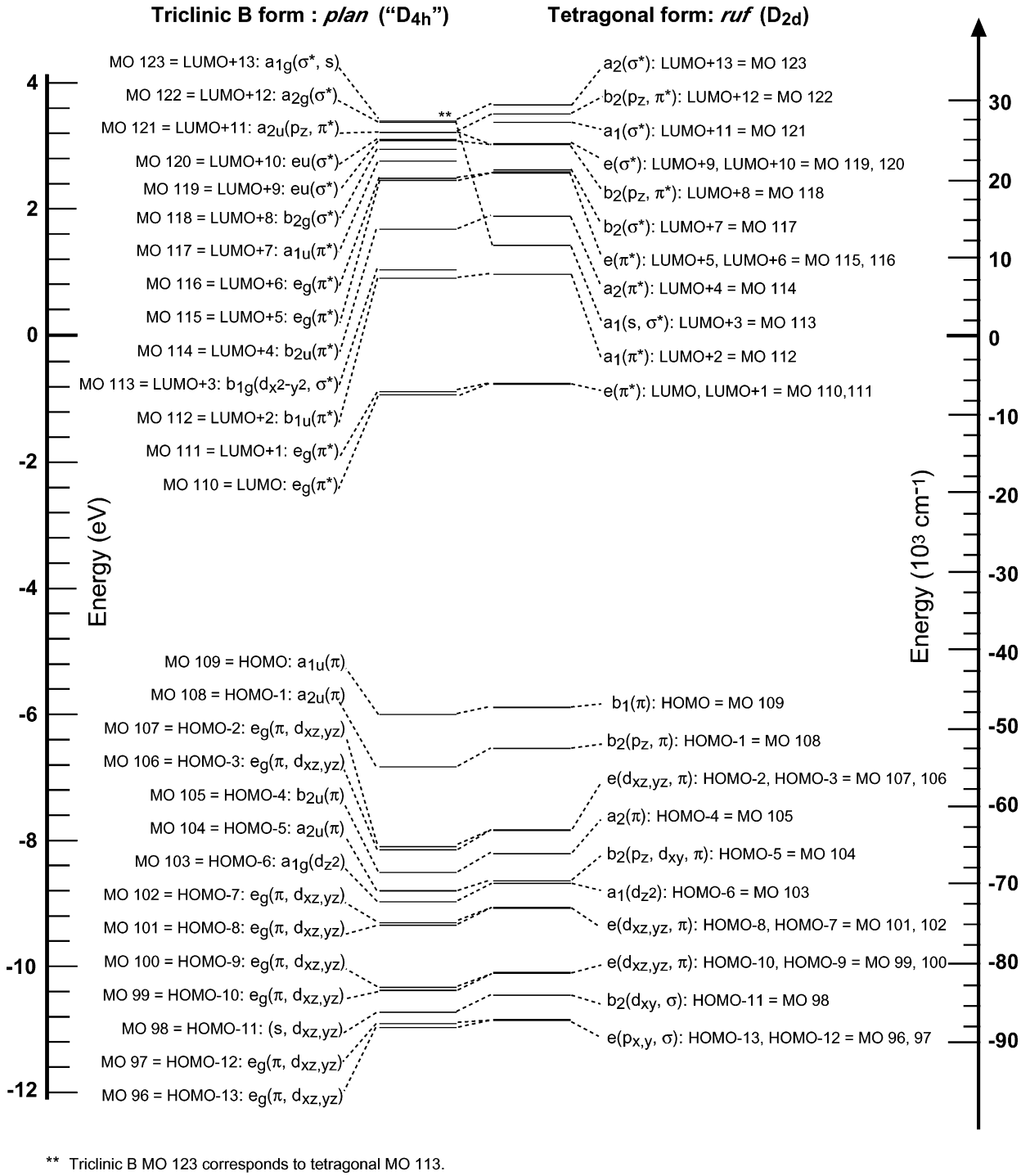

** Triclinic B MO 123 corresponds to tetragonal MO 113.

Figure 6. Selected molecular orbital energy levels for the triclinic B and tetragonal forms of NiOEP.

proposed by Gouterman[53−55] to be the source of the Q and Soret transitions. Energy levels for all 213 molecular orbitals for both the single molecule triclinic B and tetragonal forms of NiOEP are listed in Tables S1 and S3 in the Supporting Information and 28 of them nearest to the Fermi level are shown to scale in Figure 6. The most obvious result is that the *plan* orbitals are in most cases slightly lower in energy than the corresponding *ruf* orbitals. This may in general be due to the better p_z overlaps in the planar molecule than in the ruffled molecule, leading to slightly more stability in the planar orbitals. Among the four orbitals of primary interest (HOMO-1, HOMO, LUMO, and LUMO+1) the HOMO-1 has been raised over twice as high as the others from *plan* to *ruf*, as may be seen in Tables 3 and 4. This excess destabilization appears to be the source of the significant red shift in the Soret transition; it is much larger than that for the Q transitions, as was shown in Table 3. We will discuss this in detail.

A separate issue is a comparison of the degeneracy and accidental degeneracy in unsubstituted porphyrins with those found here. Orbitals equivalent to the porphyrin degenerate orbitals (such as LUMO and LUMO+1) are exactly degen-

Table 4. ZINDO-Calculated Energies of the Four Orbitals Closest to the Fermi Energy for NiP, NiOEP, and "ZnOEP" monomers

	NiOEP (*plan*), eV	NiOEP (*ruf*), eV	ΔE (*ruf*−*plan*), eV	NiP, eV	ZnOEP (*plan*),[a] eV	ZnOEP (*ruf*),[a] eV
LUMO+1	−0.886	−0.779	0.107	−1.237	−0.787	−0.680
LUMO	−0.933	−0.779	0.154	−1.247	−0.834	−0.680
HOMO	−5.994	−5.888	0.106	−6.45	−5.844	−5.732
HOMO-1	−6.829	−6.543	0.286	−7.069	−6.751	−6.456

[a] Same structure as NiOEP analogues but with Zn substituted for Ni; calculation for Zn uses no d orbitals.

erate in the *ruf* case but slightly removed from degeneracy in the *plan* case since the formal symmetry of the latter is C_i rather than D_{4h}, as seen in Table 4. The HOMO and HOMO-1 a_{1u} and a_{2u} (in D_{4h}) or b_1 and b_2 (in D_{2d}) orbitals which are accidentally degenerate in porphyrin[53−55] are clearly separate in both conformers as shown in Table 4. Walker et al.[68] find a similar separation of energies for the two highest filled MO's in OEP and attribute the separation to hyperconjugation resulting from the addition of the eight ethyl groups on the porphyrin macrocycle. To find an equivalent effect in the corresponding Ni complex, we calculated energies for NiP based upon a recent structure.[69] The results for NiP show a separation of 0.604 eV between the HOMO and HOMO-1, which are at −6.465 and −7.069 eV, respectively, as shown in Table 4. This is similar to the energy differences in the NiOEP complexes, 0.835 and 0.655 eV. The destabilization of the orbitals upon Ni complexation to porphyrin is thus similar to that found by Walker et al. upon addition of eight ethyl groups to porphyrin.[68] We find therefore that the hyperconjugation arguments used for OEP[68] may not be as significant in the nickel-complexed counterpart.

Wave Functions. The wave functions of primary interest in this paper are those involved in the state transitions Q and B. We present graphical depictions of these wave functions in an effort to identify distinctions that may underlie the differences in energies and transitions. All of the orbital transitions comprising the bulk of the state transitions (with absolute coefficients > 0.15) with one exception involve only LUMO+1, LUMO, HOMO, HOMO-1, and HOMO-4 orbitals. Figure 7 shows these 10 molecular orbitals. Note that the highly nonplanar form (*ruf*) has the more symmetrical wave functions; this reflects the exactly degenerate results found in the energy calculations and is consistent with the molecule's having exactly D_{2d} symmetry. Figures S1 and S3 in the Supporting Information each show all 28 orbitals whose energies are plotted in Figure 6, and Tables S-2 and S-4 give the detailed atomic orbital composition of these wave functions for the tetragonal (*ruf*) and triclinic B (*plan*) forms, respectively.

In Figure 7, both a top view and front view are shown for each of the principal molecular orbitals for both the *plan* and *ruf* forms. The 14° tilt of the pyrole rings in the *ruf* form is clear in the front views and even slightly evident in the top views of the MO's. It is clear that the upper two orbitals, LUMO and LUMO+1, in each form are very similar, allowing for the 90° rotation for the degenerate pair, but one difference shows up between the forms: the *plan* form has a somewhat different delocalization pattern from the *ruf* form. Both have small and nearly equal inclusion of some ethyl group orbitals.

The HOMO's are again similar, but that for the *plan* form has a clear departure from D_{4h} symmetry around the inner part of the ring but does obey the formal C_i symmetry of the complex. In addition, it has small but slightly larger contribution from ethyl orbitals than that for the *ruf* form. The HOMO-1 in the *plan* form is also similar to its *ruf* counterpart, except with C_i symmetry as in the HOMO case. The p_z overlap between the Ni and its adjacent N atoms appears to be larger in the *plan* form than in the *ruf* form. We will discuss this in greater detail later in this section. The ethyl orbitals in the *plan* form are barely perceptible and smaller than those in the *ruf* form. Both of the HOMO-4 orbitals have close to expected symmetry, but both have significant ethyl group contribution, with the *plan* form having somewhat more than the *ruf* form.

Transitions. The goal of our calculations has been to reproduce as closely as possible the experimental transitions and then to interpret the experimental results using the insights afforded by the calculations. Selected calculated monomer state transitions are shown in Table 5; tabulation of a larger set of transitions is given in Table S9 in the Supporting Information. Since, as Gouterman originally proposed,[54,70] the peaks in the experimental spectra are the linear combinations of numerous single orbital transitions, only those with coefficients greater than 0.14 (2.0% of the transition intensity), and which collectively account for at least 90% of the transition intensity, are listed in Table 5.

The calculated monomer transitions are shown in Figure 8. Since, as will be demonstrated in a later section, there is a significant amount of spectral shifting due to the solid-state environment, it would not be suitable to compare our calculated monomer results with our solid-state experimental results. Instead, we have included, where available, solution experimental values in Table 5 and Figure 8. Since solution experimental intensities were not reported, we have placed bars in Figure 8 representing the reported experimental transition energies for the *ruf* and *plan* forms of NiOEP in methylene chloride solution in the Soret region[29] and a bar representing the transition energy for an undetermined form of NiOEP in dichloromethane solution in the Q region.[67] The calculated results show excellent agreement in the Q region with the solution experimental energy, as has been observed earlier for other porphyrin ZINDO calculations.[60,71] The calculated peaks in the Soret region, however, are about 6 kcm^{-1} higher in energy than the experimental values. A similar degree of blue shift in the calculated Soret (B) transitions has been seen in numerous previous INDO

(68) Gruhn, N. E.; Lichtenberger, D. L.; Ogura, H.; Walker, F. A. *Inorg. Chem.* **1999**, *38*, 4023.
(69) Jentzen, W.; Turowskatyrk, I.; Scheidt, W. R.; Shelnutt, J. A. *Inorg. Chem.* **1996**, *35*, 3559.
(70) Gouterman, M. In *The Porphyrins;* Dolphin, D., Ed.; Academic Press: New York, 1978; p 1.
(71) Mack, J.; Stillman, M. J. *J. Porphyrins Phthalocyanines* **2001**, *5*, 67.

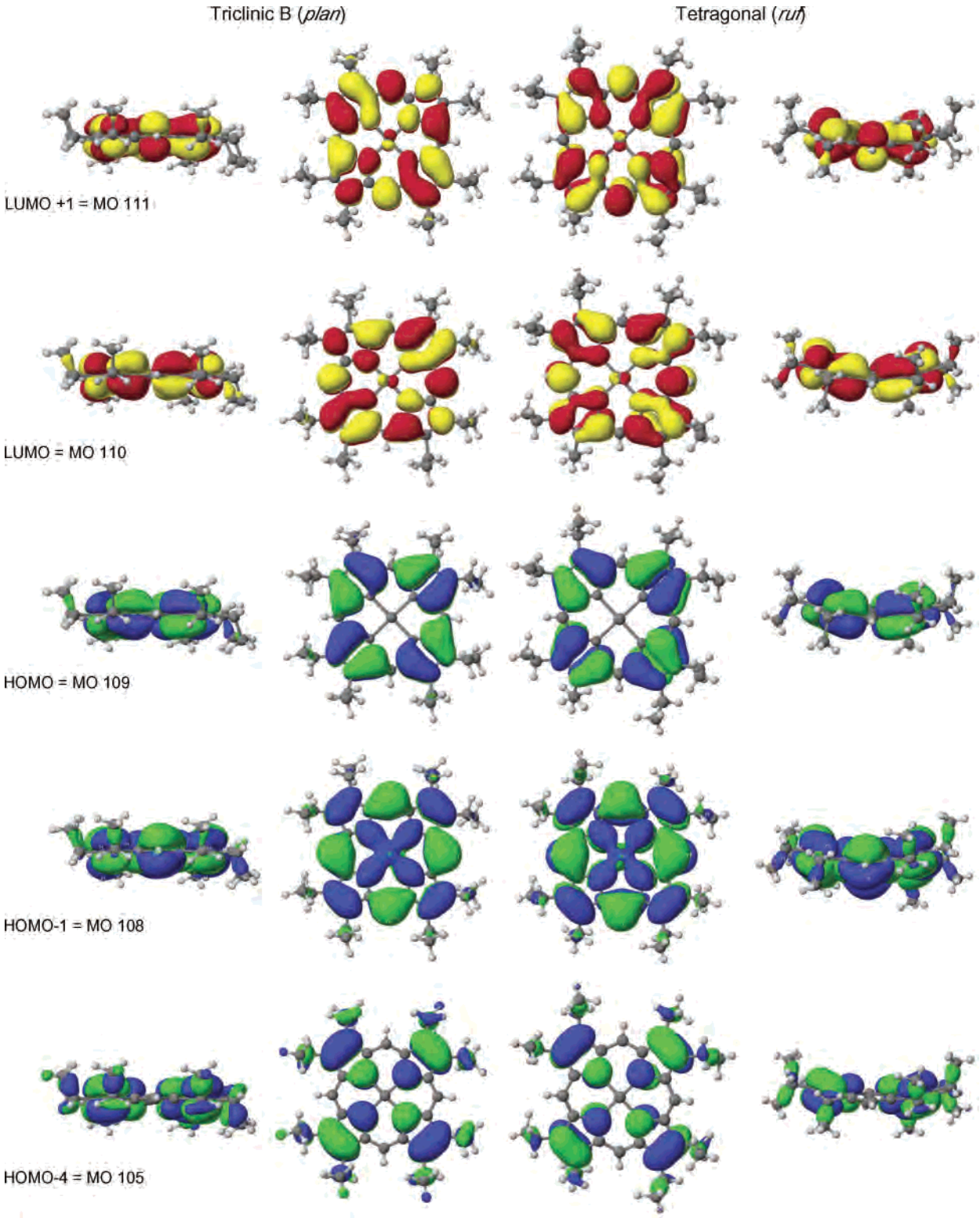

Figure 7. Selected monomer molecular orbitals for both forms of NiOEP. Both side and top views are shown for each orbital.

calculations on porphyrins: for example, several calculations with a four-orbital model produced Soret blue shifts of from 2.7 to 10.9 kcm^{-1} compared to CuP experimental spectra,[72] calculations on Fe(II)P produced transition energies that were 5−6 kcm^{-1} too high,[60] and recently calculations on ZnTPP produced a Soret transition that was 5.9 kcm^{-1} too high.[71] Despite their being higher than experiment, our calculated B energies for the *ruf* and *plan* forms do show a very similar difference (865 cm^{-1}) to that in a solution experiment (850 cm^{-1}).[29] For comparison, Shelnutt et al., using extended Huckel calculations, predicted a red shift of 410 cm^{-1} for the B peak.[29] A more complete set of experimental and

(72) Weiss, C.; Kobayashi, H.; Gouterman, M. *J. Mol. Spectrosc.* **1965**, *16*, 415.

Table 5. Selected State Transitions for NiOEP Monomers[a]

		plan form		energy (10^3cm^{-1}) {osc. strength}		*ruf* form		energy (10^3cm^{-1}) {osc. strength}	
peak	assignment (in D_{4h})	coeff	orbital transition[b]	exp	calc	coeff.	orbital transition[b]	exp	calc
Q		0.731	HOMO → LUMO	17.9[c](ref 67)	17.56	0.807	HOMO → LUMO+1		17.32
	$0.7\{a_{1u}(\pi) \rightarrow e_g(\pi^*)\}$	−0.473	HOMO-1 → LUMO+1		{0.12}	0.565	HOMO-1 → LUMO		{0.08}
	$0.3\{a_{2u}(\pi) \rightarrow e_g(\pi^*)\}$	−0.383	HOMO → LUMO+1						
		−0.27	HOMO-1 → LUMO						
		−0.725	HOMO → LUMO+1		17.68	−0.807	HOMO → LUMO		17.32
		−0.482	HOMO-1 → LUMO		{0.11}	0.565	HOMO-1 → LUMO+1		{0.08}
		−0.39	HOMO → LUMO						
		0.259	HOMO-1 → LUMO+1						
B		−0.521	HOMO-1 → LUMO	25.4 (ref 29)	31.54	0.733	HOMO-1 → LUMO+1	24.6 (ref 29)	30.77
	$0.6\{a_{2u}(\pi) \rightarrow e_g(\pi^*)\}$	0.508	HOMO-1 → LUMO+1		{2.23}	0.531	HOMO → LUMO		{2.52}
	$0.3\{a_{1u}(\pi) \rightarrow e_g(\pi^*)\}$	0.364	HOMO → LUMO+1			0.215	HOMO-1 → LUMO		
	...	0.339	HOMO → LUMO			−0.196	HOMO-4 → LUMO		
		0.336	HOMO-1 → LUMO+3						
		−0.217	HOMO-4 → LUMO						
		0.555	HOMO-1 → LUMO		31.73	−0.733	HOMO-1 → LUMO		30.77
		0.545	HOMO-1 → LUMO+1		{2.64}	0.531	HOMO → LUMO+1		{2.52}
		−0.384	HOMO → LUMO+1			0.215	HOMO-1 → LUMO+1		
		0.375	HOMO → LUMO			0.196	HOMO-4 → LUMO+1		
		−0.196	HOMO-4 → LUMO+1						
B′		0.905	HOMO-1 → LUMO+4		32.13				
	$0.8\{a_{2u}(\pi) \rightarrow b_{2u}(\pi^*)\}$	0.239	HOMO-5 → LUMO+3		{0.32}				
	...	−0.212	HOMO-1 → LUMO+1						
V		0.741	HOMO-4 → LUMO	26.2[d]	35.41	0.737	HOMO-4 → LUMO+1	26.2[d]	33.99
	$0.7\{b_{2u}(\pi) \rightarrow e_g(\pi^*)\}$	−0.389	HOMO-4 → LUMO+1	{0.030}	{0.36}	−0.372	HOMO-4 → LUMO	{0.17}	{0.27}
	$0.1\{a_{2u}(\pi) \rightarrow e_g(\pi^*)\}$	0.288	HOMO-5 → LUMO			−0.332	HOMO-5 → LUMO		
	...	0.26	HOMO-2 → LUMO+2			0.237	HOMO-1 → LUMO		
		−0.199	HOMO-1 → LUMO			−0.204	HOMO-2 → LUMO+2		
		−0.196	HOMO-5 → LUMO+1			0.193	HOMO-3 → LUMO+2		
N		0.841	HOMO-5 → LUMO	30.5[d]	39.78	−0.686	HOMO-5 → LUMO	29.2[d]	38.41
	$0.7\{a_{2u}(\pi) \rightarrow e_g(\pi^*)\}$	0.354	HOMO-4 → LUMO	{0.036}	{0.25}	−0.494	HOMO-5 → LUMO+1	{0.23}	{0.22}
	$0.1\{b_{2u}(\pi) \rightarrow e_g(\pi^*)\}$	0.226	HOMO → LUMO+5			−0.351	HOMO-4 → LUMO+1		
	...	−0.184	HOMO-4 → LUMO+1			−0.216	HOMO-4 → LUMO		
						−0.168	HOMO → LUMO+5		
L, L′		−0.755	HOMO-2 → LUMO+2	34.9[d]	49.10	−0.697	HOMO-3 → LUMO+4	35.6[d]	50.09
	see text	−0.475	HOMO → LUMO+13	{0.095}	{0.10}	−0.36	HOMO-2 → LUMO+4	{0.14}	{0.46}
		0.199	HOMO-5 → LUMO			0.307	HOMO-1 → LUMO+9		
		0.178	HOMO-1 → LUMO+6			0.182	HOMO-2 → LUMO+8		
						−0.165	HOMO-4 → LUMO+10		
						−0.158	HOMO → LUMO+5		
C						0.686	HOMO-13 → LUMO+2	30.6[d]	41.08
	$0.5\{e_g(p_{x,y},\pi) \rightarrow b_{1u}(\pi^*)\}$					−0.618	HOMO → LUMO+4	{0.007}	{0.03}
	$0.4\{a_{1u}(\pi) \rightarrow b_{2u}(\pi^*)\}$					0.192	HOMO-5 → LUMO+2		
D						−0.426	HOMO-8 → LUMO+1	34.0[d]	43.83
	$0.4\{e_g(d_{xz,yz},\pi) \rightarrow e_g(\pi^*)\}$					−0.426	HOMO-7 → LUMO	{0.013}	{0.02}
	$0.2\{e_g(d_{xz,yz},\pi) \rightarrow e_g(\pi^*)\}$					0.383	HOMO-10 → LUMO+1		
						−0.383	HOMO-9 → LUMO		
						−0.285	HOMO-1 → LUMO+4		
E						0.410	HOMO-4 → LUMO+3		48.64
	$0.5\{e_g(d_{xz,yz},\pi) \rightarrow e_g(\pi^*)\}$					−0.406	HOMO-8 → LUMO+1		{0.03}
	$0.3\{e_g(d_{xz,yz},\pi) \rightarrow e_g(\pi^*)\}$					−0.406	HOMO-7 → LUMO		
						−0.349	HOMO-10 → LUMO+1		
						−0.348	HOMO-9 → LUMO		
						0.241	HOMO-8 → LUMO		
						−0.241	HOMO-7 → LUMO+1		

[a] Only one of the two "degenerate" transitions is listed for each of transitions V, N, L, and D; see Table S9 for more complete listing of all transitions. [b] See Figure 6 for correlation of MO#, HOMO/LUMO rank, and orbital symmetry. [c] Undetermined form; most likely planar. [d] From solid-state spectra; data not available.

calculated values is listed in Table 3. This excellent agreement between solution *plan*−*ruf* red shift and our monomer calculations (based upon crystalline conformations) may not be as close as it appears if in fact Alden et al.[29] are correct regarding a lower degree of nonplanar distortion in solution than crystal.

Our assignments of several lowest-energy calculated electronic transitions are given in Table 5. Our calculated monomer transitions include not only the familiar Q and B transitions but several additional transitions that appear only in our solid-state spectra. We have reduced the detailed sets of orbital transitions for each state transition into, in most cases, a pair of principal orbital transitions (with one-significant-figure coefficients) for each assignment. Since these are from monomer calculations, we have compared the results to available Q and B solution transitions, and for other calculated transitions, we have listed our solid-state experimental results for energy comparison. The reason for being deliberate about assignments of monomer calculations is that we need to have a base from which to assign our calculated

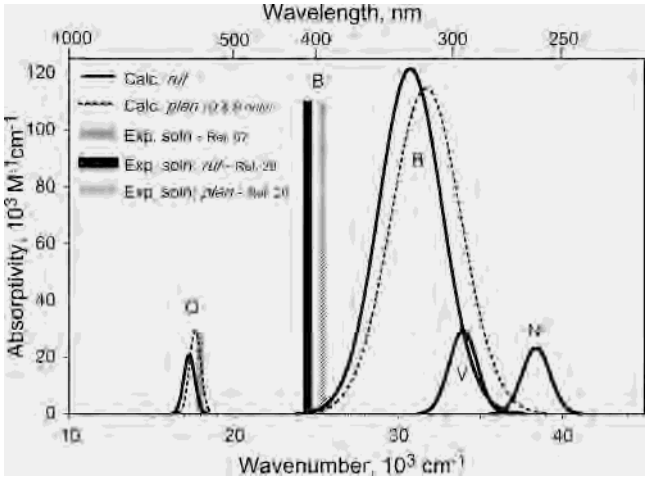

Figure 8. Calculated spectra for NiOEP monomers with solution experimental energies (sources are indicated in the figure).

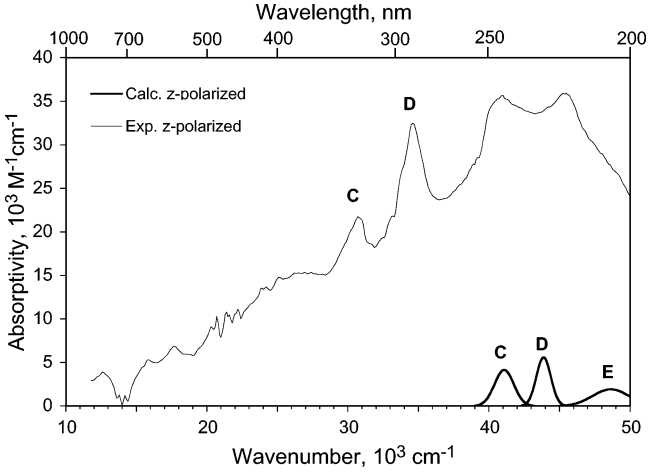

Figure 9. Experimental and calculated (monomer) z-polarized spectra for NiOEP tetragonal.

solid-state transitions, which are directly comparable to our solid-state experimental results. At least 97% of the intensity of the Q transition and from 78 to 89% of the B transition involve the same four orbitals that are the namesake of Gouterman's "four-orbital theory".[54,70]

For the most part, Table 5 is self-explanatory; we will note most items briefly, but a few need additional explanation. The calculated transitions at 17.56 and 17.68 kcm^{-1} in the *plan* form and 17.32 kcm^{-1} in the *ruf* form are pairs of transitions resulting from transitions to the degenerate or nearly degenerate LUMO and LUMO+1. The exact D_{2d} symmetry of the *ruf* form preserves the formal degeneracy of the pair. These transitions clearly correspond to the well-known Q(0,0), and we assign them as 0.7 $a_{1u}(\pi) \rightarrow e_g(\pi^*)$ and 0.3 $a_{2u}(\pi) \rightarrow e_g(\pi^*)$.

The calculated transitions at 31.54 and 31.73 kcm^{-1} in the *plan* form and at 30.77 kcm^{-1} in the *ruf* form again are pairs of transitions including components to the degenerate or nearly degenerate LUMO and LUMO+1. The components are essentially the reverse as found in Q, with B and Q each comprising essentially the same orbital transitions but in the reverse proportions (as listed in the "assignments" column of Table 5), plus several additional orbital transitions contributing about 10% of the intensity. In the first B transition in the *plan* form, however, the HOMO-1 $\rightarrow$ LUMO+3 transition which contributes about 10% of the transition intensity has no counterpart greater than 0.2% either in its "degenerate" pair or in the Q transitions. Perhaps related to this is the fact that the LUMO+3 orbital, MO 113 = b_{1g} ($d_{x^2-y^2}$, σ^*), has no counterpart in the *ruf* form below MO 124). We assign these calculated transitions as 0.6 $a_{2u}(\pi) \rightarrow e_g(\pi^*)$ and 0.3 $a_{1u}(\pi) \rightarrow e_g(\pi^*)$. The larger of the two components matches the widely accepted assignment of the B experimental peak,[53−55] and we thus assign these calculated transitions as B, even though the calculated energy is about 6 kcm^{-1} above experimental.

Peaks V and N are counterparts in the same way Q and B are. It is important to note, though, that the $a_{2u}(\pi) \rightarrow e_g(\pi^*)$ transition that is the primary one in transition N and a secondary one in transition V is not the same one as in transitions Q and B. In this case, it originates from the HOMO-5 which has more metal p_z and d_{xy} character than the HOMO-1. We thus assign the transitions as indicated in Table 5; there are no solution reports of these transitions, but we note that there are solid-state peaks about 8−9 kcm^{-1} lower in energy.

Peak L at 49−50 kcm^{-1} is somewhat an enigma; it is the only peak observed that blue shifts in going from the *plan* form to the *ruf* form, in both experiment and calculated results. Furthermore, the calculated contributing orbital transitions in the *plan* form are completely different from those in the *ruf* form. We therefore believe that the L peaks in the two forms are different: in the *plan* form L is primarily $e_g(\pi, d_{xz,yz}) \rightarrow b_{1u}(\pi^*)$ and in the *ruf* form L′ is primarily $e(\pi, d_{xz,yz}) \rightarrow a_2(\pi^*)$.

The z-polarized spectrum was calculated only for the *ruf* form and three lowest-energy transitions are shown along with the experimental z-polarized spectrum in Figure 9. The transitions are of low intensity compared with those discussed in the x,y-polarized spectrum; peak C has an ϵ_{max} of 4 $\times$ 10^3 M^{-1} cm^{-1} compared with, for instance, Q with an ϵ_{max} of 50 $\times$ 10^3 M^{-1} cm^{-1}, and thus would not be expected to appear in solution spectra. The calculated peak at 41 kcm^{-1} is about 10 kcm^{-1} higher than the experimental peak at 30.6 kcm^{-1} marked "C," but this offset is similar to that for peak B; we thus tentatively assign these transitions as shown in Table 5. We have made a similar assumption in our correlation of the 43.8 kcm^{-1} calculated peak with the experimental peak marked, D. The calculated transition at 48.64 kcm^{-1} (E) likely corresponds to an experimental transition in the 40 kcm^{-1} region, but this is less clear and we will withhold a correlation at this point.

We have thus performed detailed monomer calculations, we have assigned monomer state transitions to sets of orbital transitions and have correlated the calculated transitions to solution transitions where available. These monomer transitions will be especially helpful in assigning solid-state calculated transitions to solid-state experimental spectra.

Dimers. The purpose of the dimer calculations is to see if we can model the experimental solid-state spectra better

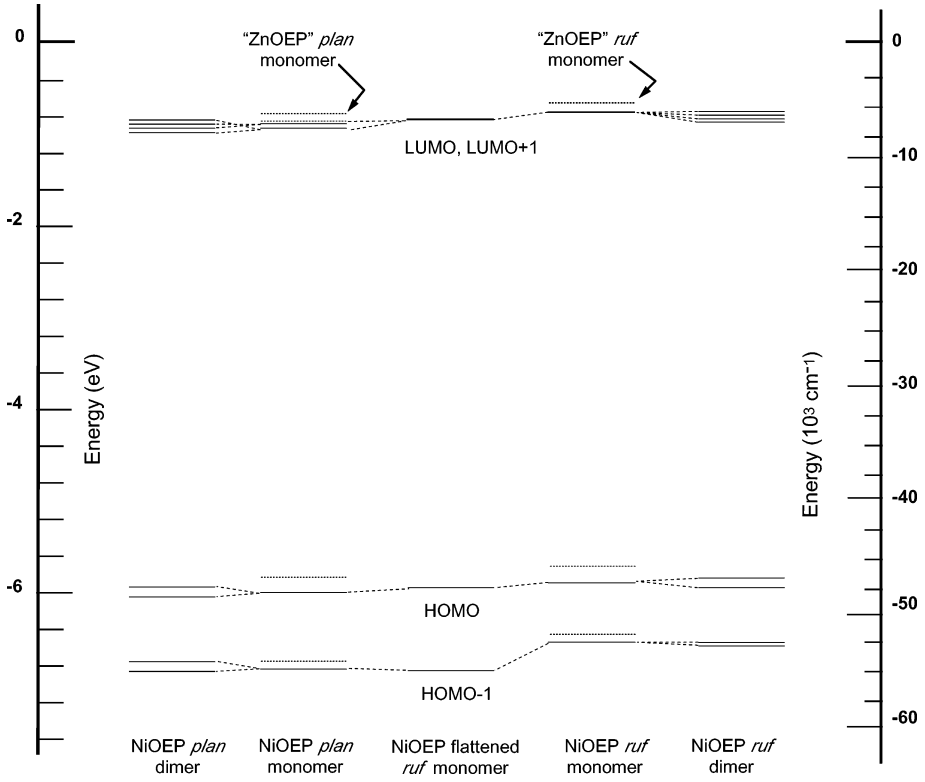

Figure 10. Selected molecular orbital energy levels for the triclinic B and tetragonal forms of NiOEP (—) and "ZnOEP" (.....).

with aggregated molecules than with monomers. (Recall, for instance, that the experimental *plan*−*ruf* red shift is 2490 cm $^{-1}$ and the calculated value for monomers is 870 cm^{-1}.) We have been successful in modeling solid-state transitions in $Ni(CN)_4^{2-}$ salts using ZINDO on both dimers and trimers in the actual crystal configuration.[47,56] In the case of Sr[Ni-$(CN)_4$)], we found that a trimer calculation can reproduce 87% of the experimental solution-to-solid-state red-shift and even a dimer can produce 47% of the trimer's perturbation.[56] We are using the CAChe implementation of ZINDO in which the maximum number of atoms calculable is 200. One NiOEP molecule has 85 atoms, thus a dimer is the maximum aggregation we could use. Based upon our results from $Ni(CN)_4^{2-}$ calculations we should see a significant portion of any perturbation with a dimer calculation. We calculated with ZINDO the effect of initial aggregation on both forms of NiOEP that we have studied.

Energies. As would be expected, the 213 orbitals calculated for the NiOEP monomers become 426 in the dimers. Complete listings of energies and selected detailed listings of wave functions are given in Tables S5−S8 in the Supporting Information. The energies of the four orbitals of primary interest are plotted to scale in Figure 10 for both monomers and dimers. In addition there are other values plotted that will be discussed later. The point to note at this juncture is that the dimer splitting of energy levels is minor compared to the energy level differences between, for instance, the HOMO and HOMO-1 levels.

Wave Functions. The relative orientations of the molecules differs from *plan* to *ruf* as shown in Figure 1 and discussed in an earlier section. The proximity of the planes (∼3.5 Å) leads one to suspect some perceptible degree of electronic and thus spectral perturbation; when Ni atoms are this close in $Ni(CN)_4^{2-}$ salts, the 8000 cm^{-1} red-shifts mentioned earlier occur.[47,56,73] The Ni atoms in NiOEP, though, are 4.80 Å apart in the triclinic B form and 8.23 Å apart in the tetragonal form so we expect no metal−metal interaction. From Figure 1, one might expect, however, metal−pyrrole ring interaction in the triclinic B (*plan*) form and pyrrole−pyrrole interaction in the tetragonal (*ruf*) form.

We have illustrated in Figure 11 two wave functions in the *ruf* form that illustrate intermolecular overlap and also serve as an example of the remarkably classic combination of monomer MO's into dimer MO's. This demonstrates a limited degree of interplanar interaction that is seen occasionally in the wave functions of dimers of both the *plan* and *ruf* forms. MO 217 is the additive combination of two monomer MO 109's and MO 218 is the subtractive combination of the same monomer MO's. The tetragonal dimer places the pyrrole rings of adjacent molecules in close proximity; there is some overlap of pyrrole π lobes leading to a joining of orbitals in the additive combination as in MO 217, while a node is retained in the subtractive combination, MO 218. Overlap occurs in other orbitals occasionally in either additive or subtractive combinations, depending upon the signs of the lobe amplitudes as shown in Figure S2, MO's 217 and 219, and in Figure S4, MO's 215, 216, 217, 219, and 220. This small degree of overlap seems to be reflected in the small separation of energies from monomer to dimer orbitals as shown in Figure 10. Metal−pyrrole π interaction was suspected in the triclinic B form, and the metal orbitals most likely to interact with orbitals on neighboring molecules

(73) Musselman, R. L.; Cornelius, J. B.; Trapp, R. M. *Inorg. Chem.* **1981**, *20,* 1931.

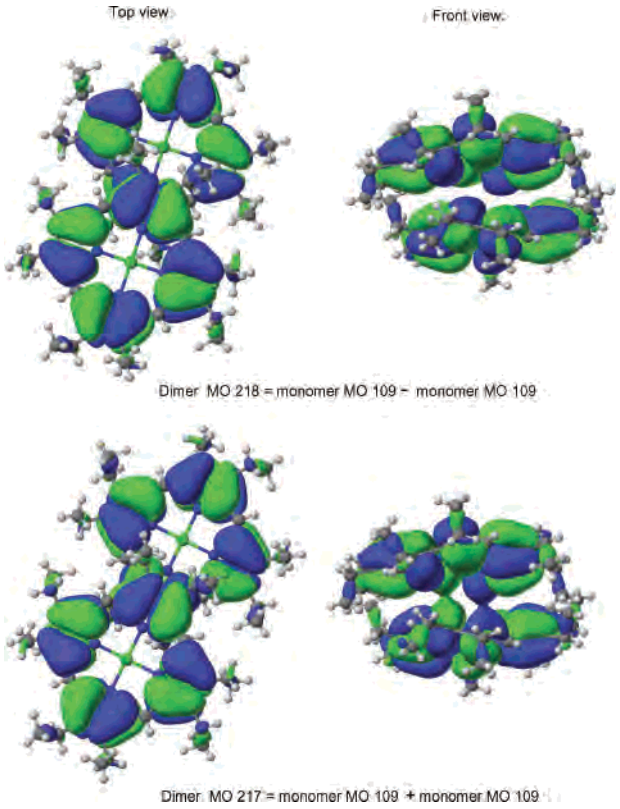

Figure 11. Example of combination of tetragonal NiOEP monomer MO's into dimer MO's with resultant intermolecular orbital overlap.

are the p_z and d_{z^2} orbitals which were found to form extended lobes along metal chains in $Ni(CN)_4^{2-}$ salts.[47,56] We see no such orbital overlap between molecules in Figure S4. In addition to intrinsic features of dimer MO's, we are interested in the origins of dimer MO's so we may assign dimer transitions as derivatives of the monomer, or standard molecular, assigned transitions such as those for Q or B. The principal monomer MO's associated with transitions Q and B are shown on the right side of Figure 12 with their correlations to dimer MO's for the tetragonal form of NiOEP. A more complete correlation diagram for both triclinic B and tetragonal forms is in Figure S5 in the Supporting Information.

Transitions. As one could have predicted, many more dimer transitions were calculated than monomer transitions. Table S10 lists the dimer calculation results and includes all transitions with at least 0.16% contribution which collectively account for at least 97% of the transition intensity and a select set for the *ruf* form is shown in Figure 12. In preparing to compare dimer transitions with monomer transitions, it is necessary to determine the monomer origins of the dimer transitions. A complete listing of dimer transitions is given in Table S10. The following is our "origin analysis" for the *ruf* transition at 17.24 kcm^{-1}, shown at the left in Figure 12. This calculated transition has numerous components, but the largest four are listed in the diagram; those transitions in red are from MO's derived from the monomer HOMO, MO 109, and those in green are MO's derived from HOMO-1, MO 108. It is clear that the red transitions from MO's 217 and 218, derived from MO 109, are more highly represented in the 17.24 kcm^{-1} transition than the green transitions from MO's 215 and 216, derived from MO 108. If all the coefficients of transitions from orbitals 217 and 218 associated with the 17.24 kcm^{-1} transition listed in Table S10 are squared and added together, they equal 0.670; likewise coefficients of transitions from orbitals 215 and 216 give 0.307. Reducing these values to one significant figure as in our assignments in Table 5 and listing the wave functions as the monomer-orbital origins, we have the following assignment for the transition at 17.24 kcm^{-1}: $0.7\{a_{1u}(\pi) \rightarrow e_g(\pi^*)\}$ and $0.3\{a_{2u}(\pi) \rightarrow e_g(\pi^*)\}$. Since this is the same assignment as Q(0,0) we may attribute this dimer transition to Q(0,0). There are actually two transitions in this region calculated for the dimer even though the monomer produced only one due to its high symmetry; the other one is at 17.29 kcm^{-1}. This multiple-transition result is expected and is discussed at length in a recent paper;[56] one of the conclusions is that the strongest transition of a multiple set in a limited aggregation will become essentially

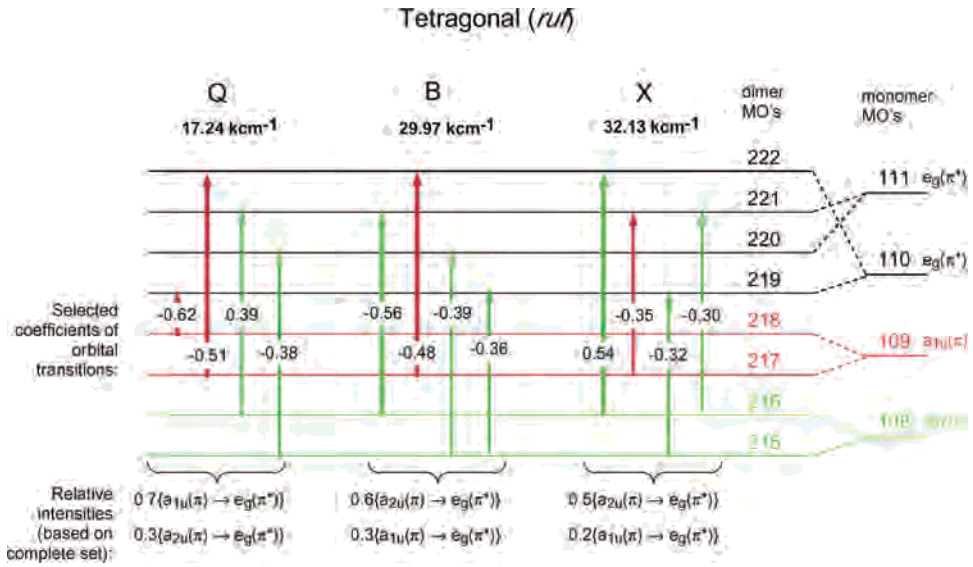

Figure 12. Selected calculated tetragonal dimer state transitions with orbital transition components and monomer orbital origins of the dimer MO's.

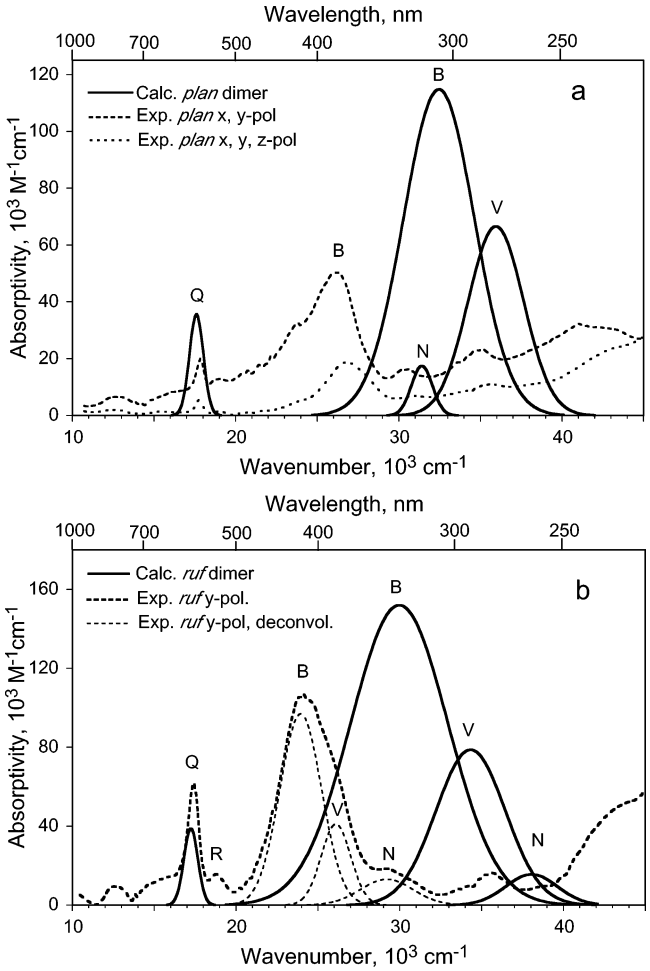

Figure 13. Calculated and experimental spectra for solid-state (or dimers) of NiOEP (a) triclinic B form (*plan*) and (b) tetragonal form (*ruf*).

the only significant one upon higher aggregation. We have made the choice therefore to select the strongest transition in a set to represent the dimer transition corresponding to the monomer transition. Thus we have chosen the 17.24 kcm^{-1} transition with an oscillator strength of 0.179 over that at 17.29 kcm^{-1} with an oscillator strength of 0.142.

The principal peak from each set of equivalent dimer state transitions, as discussed in the previous paragraph, is shown along with the polarized experimental spectra in Figure 13a,b. The correlation is equivalent to that for the monomer calculations and the solution energies. A notable exception is peak R at 18.8 kcm^{-1} in Figure 13b. This peak has been assigned previously as both the vibronic (0,1) component of Q(0,0)[54,70,74] and, based upon SCF-Xα-DOS calculations, as a separate electronic transition, unrelated to Q.[10,75−80] Since

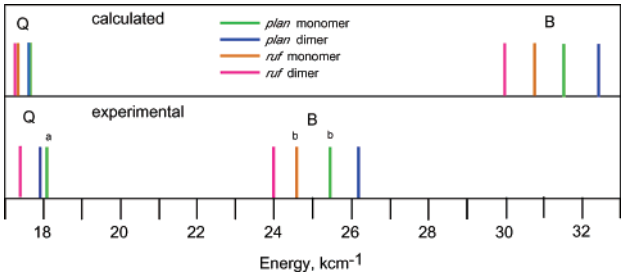

Figure 14. Energies of monomer (or solution) and dimer (or solid-state) transitions for both *plan* and *ruf* forms of NiOEP. Sources: a = ref 67; b = ref 29; all others, this work.

ZINDO did not calculate vibrational components of electronic transitions, we would have seen a transition here only if it were a unique electronic transition. No equivalent transition appears in our calculations. The conclusion from this, therefore, is that there is no significant separate electronic transition in the R region, a conclusion that agrees with the traditional peak assignment, Q(0,1). There is thus a significant discrepancy between the two calculation methods, ZINDO and X-α DOS, which we are currently exploring.

The two strongest transitions resembling the B transition are at 29.97 kcm^{-1} (osc. strength = 4.90) and at 32.13 kcm^{-1} (osc. strength = 3.56). The results of an origin analysis of these calculated transitions are shown in the middle of Figure 12. The state transition at 29.97 kcm^{-1} has orbital transitions from MO 108-derived dimer MO's (in green) predominant, the reverse of the situation for transition Q in the same diagram. Upon squaring and summing transitions from MO's 215 and 216, the fraction equals 0.598 which we have rounded to 0.6, and that for transitions deriving from MO 109 yields 0.317, rounded to 0.3. This produces the same assignment as we gave to calculated monomer transition B in Table 5, $0.6\{a_{2u}(\pi) \rightarrow e_g(\pi^*)\} + 0.3\{a_{1u}(\pi) \rightarrow e_g(\pi^*)\}$; thus this dimer transition may be assigned as B. The transition at 32.13 kcm^{-1}, X, gives similar results but has 15−20% less contribution from the orbital transitions comprising B. We had already chosen not to consider this transition as representative of B due to its smaller oscillator strength, and the less satisfactory orbital transition match is a confirmation of this choice. The selected calculated Q, B, N, and V transitions are shown along with the experimental solid-state spectra for *plan* in Figure 13a and for *ruf* in Figure 13b. As with the monomer calculations, the calculated Q transitions match experiment very well, and the calculated Soret peaks are again about 6 kcm^{-1} higher energy than experiment. Figure 14 summarizes visually the calculated and experimental dimer and monomer transition energies for both crystal forms of NiOEP that had been presented in Table 3. The similarities between equivalent values from experiment and calculations is remarkably clear in this diagram. This includes the blue shift of the *plan* solution and calculated monomer transitions upon becoming solid-state or dimerized and the red shift of the equivalent *ruf* transitions.

Solid-State Effects. Collective perturbations have been observed in other porphyrin systems as well. Aggregation

(74) Wang, M.-Y. R.; Hoffman, B. M. *J. Am. Chem. Soc.* **1984**, *106*, 4235.
(75) Kutzler, F. W.; Ellis, D. E. *J. Chem. Phys.* **1986**, *84*, 1033.
(76) Liang, X. L.; Ellis, D. E.; Gubanova, O. V.; Hoffman, B. M.; Musselman, R. L. *Int. J. Quantum Chem.* **1994**, *52*, 657.
(77) Liou, K. Y.; Newcomb, T. P.; Heagy, M. D.; Thompson, J. A.; Heuer, W. B.; Musselman, R. L.; Jacobsen, C. S.; Hoffman, B. M.; Ibers, J. A. *Inorg. Chem.* **1992**, *31*, 4517.
(78) Rende, D. E.; Heagy, M. D.; Heuer, W. M.; Liou, K.; Thompson, J. A.; Hoffman, B. M.; Musselman, R. L. *Inorg. Chem.* **1992**, *31*, 352.
(79) Murata, K.; Liou, K.; Thompson, J.; McGhee, E. M.; Rende, D. E.; Musselman, R. L.; Hoffman, B. M.; Ibers, J. A. *Inorg. Chem.* **1997**, *33*, 3363.
(80) Hoffman, C. B.; Fares, V.; Flamini, A.; Musselman, R. L. *Inorg. Chem.* **1999**, *38*, 5742.

Table 6. Selected Bond Lengths for Experimental and Modified NiOEP

	bond lengths in Å							
	tetrag (*ruf*)	triclinic (*plan*)	tetrag/tricl ratio	flattened	flat x 0.97	0.97/flat ratio	flat x 1.03	1.03/flat ratio
Ni−N1	1.93	1.945	0.992	1.93	1.872	0.970	1.988	1.030
Ni−N2	1.93	1.957	0.986	1.93	1.872	0.970	1.988	1.030
N1−C6	1.386	1.391	0.996	1.355	1.31	0.967	1.392	1.027
C6−C5	1.372	1.37	1.001	1.354	1.317	0.973	1.398	1.032
C5−C4	1.373	1.356	1.013	1.357	1.314	0.968	1.395	1.028
N2−C4	1.386	1.386	1.000	1.351	1.314	0.973	1.395	1.033
C4−C3	1.453	1.454	0.999	1.442	1.405	0.974	1.492	1.035
C3−C2	1.363	1.33	1.025	1.299	1.26	0.970	1.338	1.030
C2−C1	1.443	1.445	0.999	1.448	1.398	0.965	1.485	1.026
N2−C1	1.386	1.37	1.012	1.355	1.31	0.967	1.392	1.027

in a similar nickel porphyrin (NiUop, where Uop = uroporphyrin I)[81,82] results in a 13 nm (884 cm^{-1}) blue shift for the Soret transition and a 3 nm (98 cm^{-1}) red shift for the Q(0,0) transition.[81] Cofacial dimerization of porphyrins results in a 2500 cm^{-1} raising of the a_{1u} HOMO level above the normally equal energy a_{2u} HOMO-1 level,[83] and $\pi-\pi$ interaction between adjacent planes in solid nickel porphyrins appears to be the cause of structural changes in NiOEP[15] and NiTMP (TMP = tetramethylporphyrin).[84] Some solid-state perturbation in Ni complexes has been dramatic, with red-shifts over 8000 cm^{-1};[73] the specific crystal environment, of course, determines the degree of perturbation.[47,56]

The opposite spectral shifting of *plan* and *ruf* forms as shown in Figure 14 is the immediate cause of the much larger experimental red shift upon deformation of NiOEP in solid state vs solution.[24,29] The calculated and experimental dimer and monomer transition energies for both crystal forms of NiOEP show that changes due to aggregation are quite significant for the B peak: the blue shift upon dimerization is 820 cm^{-1} in the *plan* form and the red shift upon dimerization is 800 cm^{-1} in the *ruf* form, increasing the calculated monomer *ruf*−*plan* red shift of 870 cm^{-1} by 1620 cm^{-1} to a total *ruf*−*plan* red shift of 2490 cm^{-1}. The "solid-state" perturbation is very small for the Q(0,0) peak: there is a 20 cm^{-1} red shift in the *plan* form and an 80 cm^{-1} red shift in the *ruf* form, increasing the total monomer *ruf*−*plan* red shift by 60 cm^{-1}, from 300 to 360 cm^{-1}, again matching the experimental results. We may thus have confidence that the aggregation of NiOEP into the solid state does produce perturbations resulting in the much larger *plan*−*ruf* red shift than is observed in solution. Again, we are mindful that the monomer deformation in the tetragonal crystal may be somewhat larger than that in solution,[29] which may contribute somewhat to the enhanced red shifting of the solid-state *ruf* form.

Causes of *plan*−*ruf* Red Shifting. Now that we have demonstrated that the ruffled form of NiOEP has its Soret and Q transitions red shifted from the planar form through conformation and not necessarily as a result of deforming substituents, let us look at four final issues: (1) possible effects of the different ethyl group arrangements between the *ruf* and *plan* forms, (2) the effects of bond length changes, (3) the extent of influence of metal d orbitals, and (4) the orbital overlap consequences of deformation.

The major red shifting occurs in the Soret transition and the principal contributor to this state transition is the $a_{2u}(\pi) \rightarrow e_g(\pi^*)$ or HOMO-1 → LUMO and LUMO+1 degenerate transitions. A significant raising of the HOMO-1 orbital thus may be expected to cause the Soret transition to red shift. Our calculations as illustrated in Figures 6 and 12 show clearly that this orbital is indeed raised significantly (0.286 eV) from the *plan* form to the *ruf* form. We modified the structures to investigate specific candidates for the cause of the HOMO-1's being higher in the *ruf* form. The first modification is to retain as much of the *ruf* form as possible but simply make the porphyrin core planar. We flattened the *ruf* structure as described in the Experimental Section and obtained the energy results shown in the center column of Figure 10. The structural result is essentially a *plan* form but with the ethyl groups arranged as in the *ruf* form. The results are extremely close to the *plan* monomer energies, allowing us to conclude that the differing orientations of the ethyl groups in the *plan* and *ruf* forms do not contribute to the energy differences between the two forms nor, by extension, to the *plan*−*ruf* red shifting.

The arguments deriving from substituent-caused deformations, or that the IPNR's were the root cause of the red shift, need addressing next. The in-plane nuclear reorganizations include bond-length changes (resulting in bond-angle changes) and deformations out of the plane. We contend that out-of-plane deformations are indeed a major cause of the red shift, as we detail in a subsequent paragraph. We now, however, address the bond length issue. The variation of corresponding bond lengths from the *plan* to the *ruf* form is less than or equal to 2% (both positively and negatively), as shown in Table 6. As a test of only bond length changes and not out-of-plane deformation we looked at the effects on the HOMO-1 level of bond length changes in the flattened NiOEP *ruf* structure which, as noted earlier, had axis alignments that allowed easy modifications. We moved the Ni atom from $x = 0$, $y = 0.25$, $z = 0.125$ fractional unit cell units to $x = 0$, $y = 0$, $z = 0.125$ and then shifted the y positions of all other atoms by −0.25 units (the z values were already established from the flattening process.) We

(81) Shelnutt, J. A.; Dobry, M. M.; Satterly, J. D. *J. Phys. Chem.* **1984**, *88*, 4980.
(82) See www.chem.qmw.ac.uk/iupac/tetrapyrrole/TP/A11.html for structure.
(83) Shelnutt, J. A. *J. Phys. Chem.* **1984**, *88*, 4988.
(84) Kutzler, F. W.; Swepston, P. N.; Berkovitch-Yellin, Z.; Ellis, D. E.; Ibers, J. A. *J. Am. Chem. Soc.* **1983**, *105*, 2996.

then either expanded the positions of all atoms by 3% ("flat x 1.03") or reduced them by 3% ("flat x 0.97"). The resultant bond lengths are listed in Table 6. All lengths have been either expanded or compressed by at least 2%. The energy levels of the HOMO-1 for the three conditions were as follows: flat x 1.03 = −6.862 eV, flat = −6.843 eV, flat x 0.97 = −6.813 eV, all very close to that for the experimental *plan* structure, −6.829 eV. The HOMO-1 energy for the *ruf* structure is −6.543 eV. The maximum energy variance among the flat structures is 0.030 eV, while the difference between *ruf* and *plan* is 0.286 eV. Thus, bond length variations equivalent to those between the two experimental forms do not account for the large destabilization of the HOMO-1 in the *ruf* form.

Now we look at the effects of metal d orbitals on the spectra. Ghosh et al.[32] have proposed that a possible reason for the raising of the HOMO-1 orbital is that "a metal (d_{xy})-porphyrin (a_{2u}) antibonding interaction...is particularly effective at raising the orbital energy of the a_{2u} HOMO". We wanted to do a calculation on as similar a system as possible with the exception that no d orbitals were to be involved in order to test this proposal. In the ZINDO routine, calculations do not include Zn 3d electrons since they are remarkably low in energy.[85] We thus substituted Zn for Ni in both the *plan* and *ruf* forms and obtained the results shown in Figure 10 as "ZnOEP" with the dotted lines. In all cases, the four orbitals of primary interest are slightly higher in energy than the corresponding NiOEP, and the amount of energy increase is identical for corresponding orbitals. Thus, the enhanced raising of the HOMO-1 orbital from *plan* to *ruf* is not dependent upon metal d orbitals.

The recent comprehensive work by Shelnutt et al.[16] presents plots of planar−nonplanar red shifting as a function of ring deformation for nonmetal containing alkylporphyrins (in the body of the paper) and for Ni-containing alkylporphyrins (in their Supporting Information). The results are very similar in terms of degree of red shifting vs planar deformation, leading one to conclude that metal presence is not necessary in order to have red shifting. Shelnutt et al. have noted that nonplanarity reduces the overlap between adjacent p_z orbitals.[16] This raises somewhat the energies of orbitals, especially those that do not have nodes at or next to the interpyrrole carbons. In the *ruf* form of NiOEP, the primary functional difference from the *plan* form is the 14° twist of each pyrrole group relative to the center MN4 core plane. This forces the *meso* carbon alternately above or below the core plane, resulting in a 14° tilt between the connecting pyrrole carbon p_z orbital and the *meso* carbons's p_z orbital. Those molecular orbitals with nodes at this junction or on the *meso* carbons will not be raised in energy as much as those without a node at that location. Examining Figure 7 in detail, of the four principal orbitals, HOMO-1, HOMO, LUMO, and LUMO+1, the only one without a node at the edges of the pyrrole rings or at the *meso* carbons is the HOMO-1. It may be supposed therefore that this orbital could be raised in energy because of the reduced overlap between pyrrole p_z orbitals and the *meso* carbons.

As a final check on any contribution of metal orbitals, we notice that the metal $4p_z$ orbitals are included in the "ZnOEP" calculations as they are in the NiOEP calculations. These are visible in HOMO-1, MO108, for both forms of NiOEP in Figure 7. In the *ruf* form, the Ni p_z −N p_z overlap is perceptibly less than in the *plan* form, due to the 14° pyrrole ring tilt. This is likely a contributing factor in the raised energy of the HOMO-1 orbital in the *ruf* compared to the plan *form* and to the *plan*−*ruf* red shifting. It is clearly not a necessary factor, however, given the red shifting in nonmetal-containing porphyrins.[16]

Conclusions

This is the first demonstration of red shifting upon nonplanarity in alkylporphyrins using two pure conformations having known structures with identical substituents. We have calculated transitions of NiOEP monomers with ZINDO and have related them to published solution and vapor-state reports. We have obtained polarized absorbance spectra of single crystals of a planar and a ruffled NiOEP, and we have calculated the expected spectra of a dimer of each form. The calculated *ruf*−*plan* red shift agrees well with experiment for both monomer (solution) and dimer (solid-state) environments. We have related the solid-state spectra to the solution spectra and thus confirm the solution results. We have found that metal d orbital involvement is not a significant factor in the red shift. We believe that we have shown a clear case of red shifting in an octaalkylporphyrin due solely to a change in conformation from planar to ruffled.

Acknowledgment. The authors are grateful to the National Science Foundation for an instrumentation grant to R.L.M. (CHE 9203392) and to the Howard Hughes Medical Institute and the Franklin and Marshall College Hackman Fund for research fellowships to J.S.E. We thank Professors Richard Moog, James Spencer, Jay Anderson, and Scott Van Arman of Franklin and Marshall College for helpful discussions. We are also grateful to the reviewers who have made helpful suggestions.

Supporting Information Available: Graphical and numeric depictions of wave functions, energies of all wave functions, tables of orbital transition components, and parameters of calculated state transitions. This material is available free of charge via the Internet at http://pubs.acs.org.

Note Added after ASAP Posting

This article was released ASAP on 8/12/04 with some minor errors in Table 3. The corrected version was posted on 8/19/04.

IC0496931

(85) Mann, J. B.; Meek, T. L.; Knight, E. T.; Capitani, J. F.; Allen, L. C. *J. Am. Chem. Soc.* **2000**, *122*, 5132.